Geometric Mechanics: the 1:1:2 and 1:2:2 resonances

Group 20: Javier Chico Vazquez, Michal Fedorowicz,

Francesco Piatti, Max Raso & Christopher Vargas

Supervised by Prof. Darryl D. Holm

Department of Mathematics, Imperial College London

June 2021

Contents

1 Abstract

The aim of the present paper is to introduce the 1:1:2 with the elastic spherical pendulum as motivation, a physical system of great interest in itself as it possesses deep properties such as monodromy, the stepwise precession of the swing plane and further results stochastic in nature. An approximate formula for the stepwise precession angle was obtained. Furthermore, the 1:2:2 resonance was explored with the aide of normal forms and comparisons were drawn between both systems. Moreover, a wide range of applications of the results were considered, namely the elastic Foucault pendulum.

Please find all the Python code here: `https://github.com/cv319/M2R20-Repository`

2 Introduction to the elastic spherical pendulum and Lagrangian Mechanics

The driving influence for this research project is to study the elastic spherical pendulum, its 1:1:2 resonance and compare it to the 1:2:2 resonance. The main tools used to do so are techniques from Lagrangian and Hamiltonian Mechanics, which will now be introduced.

2.1 A very brief introduction to Lagrangian and Hamiltonian Mechanics

To begin with we define the Lagrangian of a system, $\mathcal{L}$, as the difference between the kinetic and potential energy (K and U respectively) (1).

$$\mathcal{L}(t, x, y, z, \dot{x}, \dot{y}, \dot{z}) := K - U$$

Using the Lagrangian we can define the action as the integral of the Lagrangian over a certain trajectory (2),

$$S := \int \mathcal{L} dt$$

Hamilton's principle, also known as the principle of least action, says that the trajectory the system follows minimizes the action (1, 2), i.e.

$$\delta S = \delta \int \mathcal{L} dt = 0$$

we can find out the trajectory using results from Variational Calculus, namely the Euler-Lagrange equations, dictating the path the trajectory follows.

$$\frac{d}{dt}\left(\frac{\partial \mathcal{L}}{d\dot{x}}\right) = \frac{\partial \mathcal{L}}{\partial x}$$

and similar for the other independent coordinates, getting n equations of order 2 for the whole system for a single particle. In most cases $n = 3$. These, along the initial conditions, define the equations of motion. It must be noted that the Euler-Lagrange equations produce extrema of the action, not necessarily minima, but for most physical systems the trajectories are indeed minima. Moreover, when the potential is only a function of position they are equivalent to Newton's equations of motion (2). Building from the above section, and by defining the Hamiltonian as the Legendre transform of the Lagrangian (1), we can get an alternative form of the equations of motion:

$$H = \sum_i p_{x_i} \dot{x}_i - \mathcal{L}$$

With $p_{x_i} = \frac{\partial \mathcal{L}}{\partial \dot{x_i}}$ the momentum canonical to each coordinate. The equations of motion now become a system of differential equations of first order, but we will have twice as many as in the Lagrangian formulation. They are (2):

$$\dot{p}_{x_i} = \frac{\partial H}{\partial x_i} \qquad\qquad \dot{x}_i = -\frac{\partial H}{\partial p_{x_i}}$$

Define the position vector $\mathbf{x} = (x_1, x_2, ..., x_n)$ and vector of momenta $\mathbf{p} = (p_{x_1}, p_{x_2}, ..., p_{x_n})$. One can now define Poisson Brackets for any functions A, B of position and momenta (1):

$$\{A, B\} = \frac{\partial A}{\partial \mathbf{x}} \frac{\partial B}{\partial \mathbf{p}} - \frac{\partial B}{\partial \mathbf{x}} \frac{\partial A}{\partial \mathbf{p}}$$

For time independent hamiltonians we have $\dot{H} = \{H, H\} = 0$ (1).

3 1:1:2 resonance

Consider a physical system consisting of a mass m suspended from a fixed point on a massless elastic spring which obeys Hooke's law, a diagram is available in Figure 1. Let l_0 be the length of unstretched spring and k denote its spring constant. Let $\mathbf{X} = (X, Y, Z)$ be the position of the mass in coordinates centered

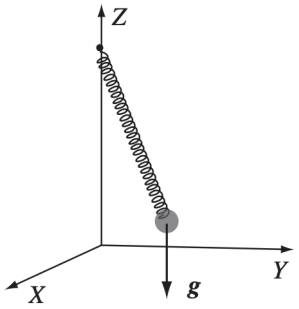

(a) Obtained from (1 p. 292)

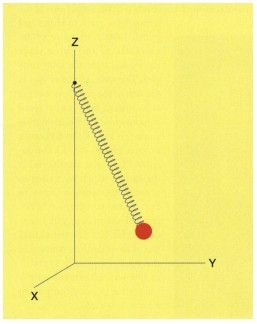

(b) Obtained from (3 p.611)

Figure 1: A diagram of the elastic spherical pendulum

around the point to which the spring is attached. Then its velocity is given by $\dot{\mathbf{X}} = (\dot{X}, \dot{Y}, \dot{Z})$. Hence the total kinetic energy of the mass is $E_k = \frac{m}{2}|\dot{\mathbf{X}}|^2$. There are two forces acting on the mass: gravity and the elastic force. These forces can be thought of as gradients of gravitational potential and potential energy of the spring respectively. The gravitational potential of the mass is $V_g = mgZ$ and potential energy of the spring is $V_s = \frac{k}{2}(|\mathbf{X}| - l_0)^2$ (it is 0 when spring is in the unstretched position). Hence the Lagrangian for

our system can be expressed as (in line with the results from (1]):

$$\mathcal{L} = \frac{m}{2}|\dot{\mathbf{X}}|^2 - mgZ - \frac{k}{2}\left(|\mathbf{X}| - l_0\right)^2$$

As in (1) we will assume small perturbations from the equilibrium position i.e. $|X - l_0\mathbf{e}_3| = l_0\epsilon$, $\epsilon \ll 1$. Let (x, y, z) be coordinates of the mass with $\mathbf{x} = (x, y, z) = (X, Y, Z - l_0) = \mathbf{X} - l_0\mathbf{e}_3$ (i.e. we move the centre of our coordinate system by l_0 in the downward direction). The small perturbation assumption then reads $\frac{|\mathbf{x}|}{l_0} = \epsilon \ll 1$. The potential energy of the spring then becomes:

$$V_s = \frac{k}{2}\left(|\mathbf{X}| - l_0\right)^2 = \frac{kl_0^2}{2}\left(\left|\frac{\mathbf{x}}{l_0} + \mathbf{e}_3\right| - 1\right)^2 = \frac{kl_0^2}{2}\left(\left|\left(\frac{x}{l_0}, \frac{y}{l_0}, \frac{z}{l_0} + 1\right)\right| - 1\right)^2 = \frac{kl_0^2}{2}\left(\sqrt{1 + \frac{2z}{l_0} + \frac{|\mathbf{x}|^2}{l_0^2}} - 1\right)^2.$$

As in (1) we can approximate this expression using a Taylor expansion: $\sqrt{1+a} = 1 + \frac{a}{2} - \frac{a^2}{8} + O(a^3)$ with $a = \frac{2z}{l_0} + \frac{|\mathbf{x}|^2}{l_0^2} = O(\epsilon)$, as $\frac{|\mathbf{x}|^2}{l_0^2} = \epsilon^2$ and $\frac{z}{l_0} < \frac{\mathbf{x}}{l_0} = \epsilon$

$$V_s = \frac{kl_0^2}{2}\left(\sqrt{1 + \frac{2z}{l_0} + \frac{|\mathbf{x}|^2}{l_0^2}} - 1\right)^2 = \frac{kl_0^2}{2}\left(\frac{z^2}{l_0^2} + \frac{z(x^2+y^2)}{l_0^3} + o(\epsilon^3)\right).$$

(please find detailed steps in *Appendix*). We will now approximate the gravitational potential as in (1). Let θ be the angle between z-axis in the downward direction and spring. Then $Z \approx l_0(1 - \cos(\theta))$, as we are assuming small perturbations from the unstretched position. Then the gravitational potential becomes $V_g \approx mgl_0\left(1 - \cos(\theta)\right)$, which can be further approximated using $\cos(a) = 1 - \frac{a^2}{2} + O(a^4)$ and $a = \theta$. As we are assuming small perturbations we have $\theta \approx \sqrt{\sin(\theta)^2} \approx \sqrt{\frac{x^2+y^2}{l_0^2}} = O(\epsilon)$. Hence we obtain

$$V_g \approx mgl_0\left(\frac{\theta^2}{2} + O(\epsilon^4)\right) \approx mg\left(\frac{x^2+y^2}{2l_0} + o(\epsilon^3)\right).$$

Combining above approximations of potentials we obtain cubic approximation of the Lagrangian (as in (1,4)):

$$\frac{L}{m} = \frac{1}{2}\left(\dot{x}^2 + \dot{y}^2 + \dot{z}^2\right) - \frac{1}{2}\left(\omega_R^2\left(x^2+y^2\right) + \omega_Z^2 z^2\right) + \frac{1}{2}\lambda\left(x^2+y^2\right)z,$$

with $\omega_R = \sqrt{\frac{g}{l_0}}$, $\omega_Z = \sqrt{\frac{k}{m}}$ and $\lambda = l_0\frac{\omega_Z^2}{l^2}$ in line with (4).
Euler-Lagrange equations for this cubic approximation are (1,4):

$$\ddot{x} + \omega_R^2 x = \lambda xz \qquad \ddot{y} + \omega_R^2 y = \lambda yz \qquad \ddot{z} + \omega_Z^2 z = \frac{1}{2}\lambda(x^2 + y^2)$$

3.1 Average Lagrangian and Average Euler-Lagrange equations

We now want to represent this dynamical system as the product of a *slowly varying complex amplitude* times a *rapidly varying phase factor* in order to produce the so called **slowly varying envelope (SVE)** approximation. To do so, we make use of the averaged Lagrangian technique (1,4,5) where the solution of (5.2.21) is assumed to be of the 1:1:2 form (i.e. $\omega_Z = 2\omega_R$):

$$x = \Re[a(t)\exp(i\omega_R t)] \qquad y = \Re[b(t)\exp(i\omega_R t)] \qquad z = \Re[c(t)\exp(2i\omega_R t)]$$

Here, the complex coefficients $a(t)$, $b(t)$, $c(t)$ are assumed to vary on a time scale which is considerably longer than the period of the oscillations. First step is substituting into L_{112}/m, then we use our small period assumption, meaning that all the terms containing a complex exponential will integrate to zero when calculating the action, so they are negligible in terms of the Euler Lagrange equations and are hence removed. Furthermore, as a, b, c are assumed to vary slowly, terms with a derivative to the second power or higher are also ignored. Please, see *Appendix* for full calculations. The remaining terms, after combining complex conjugates, give us the final form of the average Lagrangian (1, 4):

$$\langle L \rangle = \frac{1}{2}\omega_R[\Im(\dot{a}a^* + \dot{b}b^* + 2\dot{c}c^*) + \Re(\kappa(a^2 + b^2)c^*)] \tag{3.1}$$

Average Euler-Lagrange can be derived by treating the envelope variables as generalised coordinates, setting:

$$\frac{d}{dt}\left(\frac{\partial\langle L\rangle}{\partial\dot{q}^*}\right) = \frac{\partial\langle L\rangle}{\partial q^*} \qquad \text{for} \quad q = a, b, c$$

we obtain the SVE equations (1, 4):

$$i\dot{a} = \kappa a^* c \qquad i\dot{b} = \kappa b^* c \qquad i\dot{c} = \frac{\kappa}{4}(a^2 + b^2) \tag{3.2}$$

3.2 Three-wave interaction equations

Consider a linear change of variables as in (1):

$$A = \frac{1}{2}\kappa(a + ib) \qquad B = \frac{1}{2}\kappa(a - ib) \qquad C = \kappa c$$

The three wave equations then take the form (1, 4):

$$i\dot{A} = B^*C \qquad i\dot{B} = A^*C \qquad i\dot{C} = AB \tag{3.3}$$

We can use a method based on Noether's Theorem as stated in chapter 6 of (2) to find a constant of motion of this system. Applications of these equations will be given at the end of the report.

Theorem 3.1. ***Noether's Theorem*** *(2) For each symmetry of the Lagrangian, there is a conserved quantity. Furthermore if the Lagrangian is invariant, to first order in the small number ϵ, under the change of coordinates, $q_i \to q_i + \epsilon K_i(q)$, where each $K_i(q)$ may be a function of all q_i, then $P = \sum_i \frac{\partial L}{\partial \dot{q}_i} K_i(q)$ is conserved.*

We can use the above theorem to find constants of motion for our system. The averaged Lagrangian is invariant under the following changes of variables: $S : \begin{pmatrix} a \\ b \\ c \end{pmatrix} \to \begin{pmatrix} ae^{i\epsilon} \\ be^{i\epsilon} \\ ce^{2i\epsilon} \end{pmatrix}$ and this change of variables is equivalent to $\begin{pmatrix} A \\ B \\ C \end{pmatrix} \to \begin{pmatrix} Ae^{i\epsilon} \\ Be^{i\epsilon} \\ Ce^{2i\epsilon} \end{pmatrix}$. Linearisation of S yields linear change of variables:

$$\begin{pmatrix} A \\ B \\ C \end{pmatrix} \to \begin{pmatrix} A + \epsilon \frac{d}{d\epsilon}(Ae^{i\epsilon})|_{\epsilon=0} \\ B + \epsilon \frac{d}{d\epsilon}(Be^{i\epsilon})|_{\epsilon=0} \\ C + \epsilon \frac{d}{d\epsilon}(Ce^{2i\epsilon})|_{\epsilon=0} \end{pmatrix} = \begin{pmatrix} A + \epsilon K_A \\ B + \epsilon K_B \\ C + \epsilon K_C \end{pmatrix}, \qquad \text{with } K_A = iA,\ K_C = iB,\ K_C = 2iC.$$

Hence we have a conserved quantity

$$N = \frac{\partial L}{\partial \dot{A}} K_A + \frac{\partial L}{\partial \dot{B}} K_B + \frac{\partial L}{\partial \dot{C}} K_B = \left(\frac{\partial L}{\partial \dot{a}} \frac{\partial \dot{a}}{\partial \dot{A}} + \frac{\partial L}{\partial \dot{b}} \frac{\partial \dot{b}}{\partial \dot{A}} \right) K_A + \left(\frac{\partial L}{\partial \dot{a}} \frac{\partial \dot{a}}{\partial \dot{B}} + \frac{\partial L}{\partial \dot{b}} \frac{\partial \dot{b}}{\partial \dot{B}} \right) K_B + \frac{\partial L}{\partial \dot{c}} \frac{\partial \dot{c}}{\partial \dot{C}} K_C.$$

After substituting values of partial derivatives and K_A, K_B, K_C we find that

$$|A|^2 + |B|^2 + 2|C|^2 = const.$$

Using the three wave equations we can also notice that:

$$\frac{d}{dt}|A|^2 = \frac{dA}{dt}A^* + \frac{dA^*}{dt}A = \frac{A^*B^*C}{i} - \frac{ABC^*}{i} = \frac{\Im(A^*B^*C)}{2}.$$

Similarly we find that

$$\frac{d}{dt}|B|^2 = \frac{\Im(A^*B^*C)}{2}, \qquad \Longrightarrow \qquad \frac{d}{dt}\left(|A|^2 - |B|^2\right) = 0,$$

hence $|A|^2 - |B|^2$ is another constant of motion. Also, the Lagrangian has no explicit time dependence hence the energy in the system is conserved ((2), chapter 6), which means that the Hamiltonian $H = \frac{|a|^2}{2} + \frac{|b|^2}{2} + 2|c^2| - \frac{\lambda}{8}\Re((a^2+b^2)c^*) + \frac{1}{2}\Im(\dot{a}a^* + \dot{b}b^* + 2\dot{c}c^*)$ is constant on any given trajectory. But $\frac{|a|^2}{2} + \frac{|b|^2}{2} + 2|c^2| = |A|^2 + |B|^2 + 2|C|^2$ is a constant of motion and $\Im(\dot{a}a^* + \dot{b}b^* + 2\dot{c}c^*) = \frac{3\kappa}{2}\Re((a^2+b^2)c^*)$. We also have that $ABC^* = \frac{\kappa^3}{4}(a^2+b^2)c^*$. Hence $K = \Re(ABC^*)$ is a constant of motion. (Find detailed calculations in the appendix). Hence following quantities are found to be constant (1):

$$K = \Re(ABC^*)$$

$$N = |A|^2 + |B|^2 + 2|C|^2$$

$$J = |A|^2 - |B|^2.$$

The symmetries corresponding to J and N are:

$$\begin{pmatrix} A \\ B \\ C \end{pmatrix} \to \begin{pmatrix} Ae^{i\epsilon} \\ Be^{i\epsilon} \\ Ce^{2i\epsilon} \end{pmatrix} \text{ and } \begin{pmatrix} A \\ B \\ C \end{pmatrix} \to \begin{pmatrix} Ae^{i\epsilon} \\ Be^{-i\epsilon} \\ C \end{pmatrix} \quad \text{respectively, and they both leave Hamiltonian invariant (1).}$$

3.3 Numerical results for the 1:1:2 resonance and evaluation of the slowly varying envelope approximation (SVE)

The aim of this section is to simulate the original and approximate equations to verify numerically the precession of the swing plane as well as ensure the SVE equations are a precise approximation. To ensure pure resonance (4) the parameters were set to:

$$g = \pi^2 \quad l = 1 \quad m = 1 \quad k = 4\pi^2$$

and with initial conditions as prescribed in (4):

$$(x_0, y_0, z_0) = (0.006, 0, 0.012) \quad (\dot{x_0}, \dot{y_0}, \dot{z_0}) = (0, 0.00489, 0)$$

The equations were integrated with the built in integrator from `SciPy` a powerful scientific computing package (6). The python `NumPy` (7) was also widely used to improve the performance of the code. with the above parameter values tuned by Holm et al. in 2002 (4) to ensure the figure is aesthetic. Other integration methods specialized for problems arising from geometric mechanics (8) could also be fitting. The system was simulated for 1000 seconds, and the projection onto the $x - y$ plane was plotted in Figure 2. Moreover, for the envelope equations, each one was expanded into real and imaginary parts, giving six real equations which are the ones actually integrated. The initial conditions for a_0, b_0, c_0 are the following (4):

$$\alpha_0 = \arctan\left(-\frac{\dot{x}_0}{\omega_R x_0}\right) \quad \beta_0 = \arctan\left(-\frac{\dot{y}_0}{\omega_R y_0}\right) \quad \gamma_0 = \arctan\left(-\frac{\dot{z}_0}{2\omega_R z_0}\right)$$

$$|a_0| = \frac{x_0}{\cos\alpha_0} \quad |b_0| = \frac{-\dot{y}_0}{\omega_R \sin\beta_0} \quad |c_0| = \frac{z_0}{\cos\gamma_0}$$

with

$$a_0 = |a_0|\exp(i\alpha_0) \quad b_0 = |b_0|\exp(i\beta_0) \quad c_0 = |c_0|\exp(i\gamma_0)$$

For a derivation of this equations for the initial conditions of a_0, b_0 and c_0 please visit the *Appendix* in its corresponding subsection. Once the initial conditions are set, the simulations to observe the stepwise precession are conducted. The phenomenon is on display on Figure 2, where it is clear both figures are very close, almost indistinguishable, meaning the slowly varying envelope approximations work well.

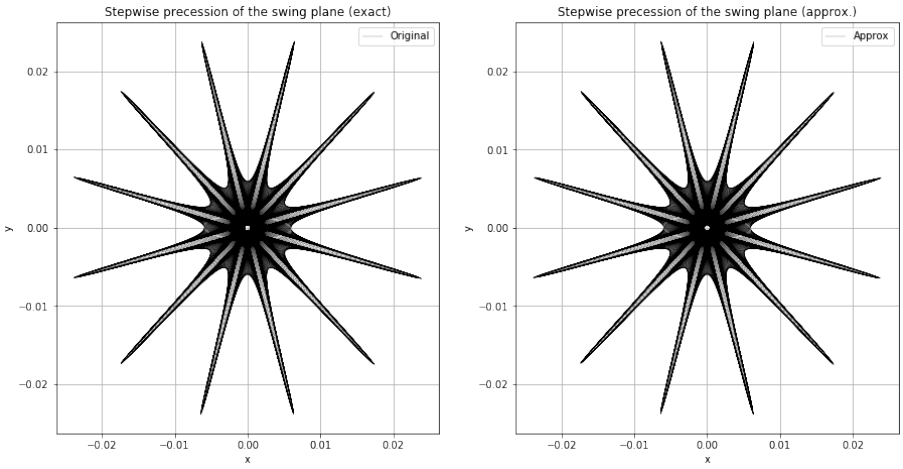

Figure 2: The stepwise precession of the swing plane. Original equations to the left, SVE to the right, and both plots are indistinguishable. System simulated for 1000 seconds.

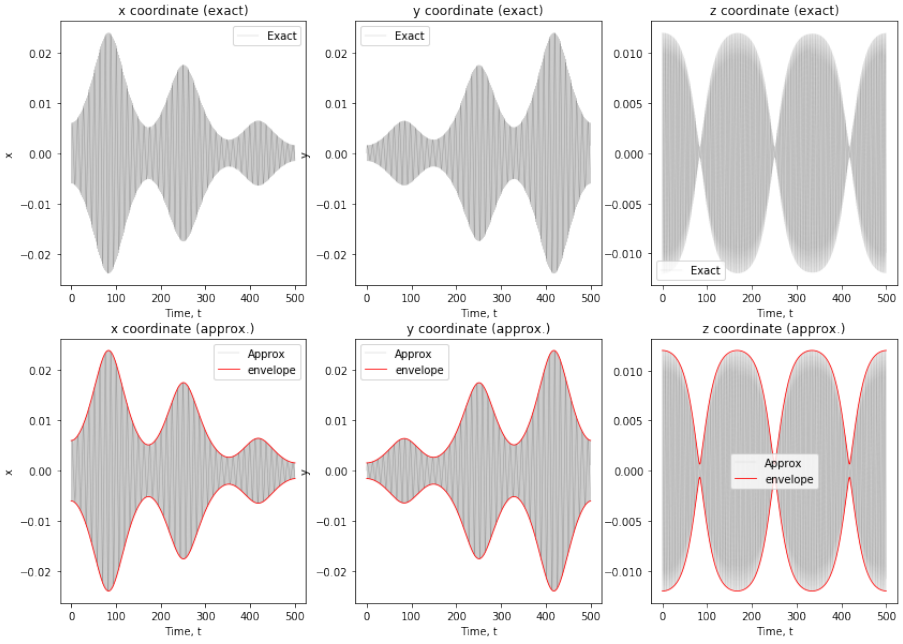

Figure 3: Above the exact equations, below the SVE equations. The SVE approximation matches the exact equations almost to machine precision.

In Figure 3 we compare the individual coordinates as well, this time simulated for half the time, 500 seconds, with the same initial conditions and physical parameters. Once again, it is clear the SVE equations match the exact equations and furthermore the red curves (which are $\pm|a(t)|, \pm|b(t)|$ and $\pm|c(t)|$) also perfectly "envelope" the curves as expected from their definition.

Recurrencies Another interesting observation from Figure 3 are the recurrencies evidenced, similar to those discussed by Verhulst in (9): maxima of the envelope for z occur when both the envelopes for x and y are close to zero, and similarly maxima of x and y occur when z is close to zero. This suggest an exchange of energy between the coordinates: as energy is conserved (1), when it is being used to gain gravitational potential it can not also be used for the elastic potential and this interplay can be visualized in Figure 3.

A similar recurrence also takes place between the x and y coordinates, this case at the maxima of their respective envelopes (which coincide): only so much energy can be used to reach the maxima and it must be distributed between both coordinates. As the pendulum precesses around the origin Figure 3 shows how the energy is distributed between the planar coordinates at the maxima. Furthermore, this is just a different way of visualizing the precession, as we can see how the motion travels through the plane by considering the values of the x and y coordinates.

3.4 A Brief note on Monodromy

Monodromy characterises a singularity in the phase-space manifold of a Hamiltonian system. This singularity precludes a global definition of canonical phase-space variables, information an interested reader can learn more about in (10). Often, we choose to observe monodromy as the obstruction to globally-defined, unique action-angle variables (11). This idea was first made explicit in complex analysis, where examples of analytic continuation, for certain analytic $F(z)$, gave different values upon arrival to the initial point. One such example being the square-root function in the complex plane. (Figure 4)

3.4.1 Swinging Pendulum

Over time, we have observed monodromy in countless different physical systems, with action-angle variables obstructing uniqueness along certain monodromy circuits. These, now multi-valued, action and angle functions contain branch points which are key to understanding our elastic spherical pendulum system. Consider a closed circuit surrounding a branch point. Following these action-angle variables around such a circuit, corresponds to reaching a different state of the system. This can lead to families of classical paths, changing their topological structure as they travel along said monodromy circuits. With each swing of our pendulum, this topological displacement means our "bob" eventually transits the region near the singular equilibrium position, causing this step-wise precision (change in the swinging plane) (10).

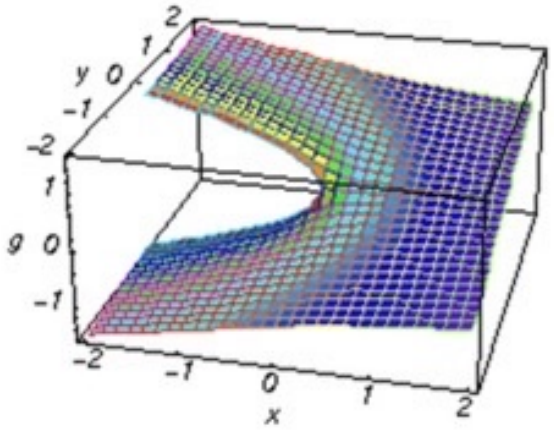

Figure 4: Monodromy for the square-root function in the complex plane. (Obtained from (12))

4 An approximate formula for the stepwise precession angle

The aim of this section is to seek a similarity solution for the stepwise precession angle, by using dimensional analysis, the Buckingham's Pi-Theorem and techniques from statistics. We perform dimensional analysis to find dimensionless groups (13). For the sake of brevity, assume as before that $y_0 = 0$ and $\dot{x}_0 = \dot{z}_0 = 0$. Then 7 relevant variables are identified:

$$\{g, l, k, m, \dot{y_0}, x_0, z_0\}$$

where l is the length of the spring at the equilibrium position. Furthermore, pure resonance (1:1:2) is imposed, which gives us:

$$2\omega_R = \omega_Z \Longrightarrow \frac{g}{l} = \frac{k}{m}$$

Moreover, we have that at the equilibrium position

$$l = l_0 + \frac{mg}{k}$$

where l_0 is the length of the unstretched string. Combining those two equations:

$$l = l_0 + \frac{l}{4} \Longrightarrow l_0 = \frac{3}{4}l$$

Performing dimensional analysis on the relationship $\theta = f(g, l, k, m, \dot{y_0}, x_0, z_0)$, and assuming

$$\theta_{\text{prec}} = g^a l^b k^c m^d \dot{y_0}^e x_0^f z_0^g$$

equating the dimensions of both sides (recall angles are non-dimensional quantities), and applying Buckingham's Pi-Theorem (13),

$$1 = L^a T^{-2a} L^b M^c T^{-2c} M^d L^e T^{-e} L^f L^g$$

three independent linear equations are obtained, one for each physical dimension:

$$0 = a + b + e + f + g \qquad 0 = -2a - 2c - e \qquad 0 = c + d$$

the second equation informs that the relevant quantity for k and m is their ratio, not each quantity individually. However this ratio is proportional to g/l, and thus we can ignore k and m, as they will not be

independent of g and l. This is further reinforced by noting that the original differential equations depend on ω_R and λ, which depend solely on g and l when pure resonance is imposed, and hence it is reasonable to take $c = 0$, and thus the equations become

$$e = -2a \qquad 0 = a + b - 2a + f + g \Longrightarrow g = a - b - f$$

solving them, the problem is reduced to:

$$\theta_{\text{prec}} = g^a l^b \dot{y_0}^{-2a} x_0^f z_0^{a-b-f} = \left(\frac{g z_0}{\dot{y_0}^2}\right)^a \left(\frac{l}{z_0}\right)^b \left(\frac{x_0}{z_0}\right)^d$$

and we find the following dimensionless groups:

$$\eta_1 = \frac{g z_0}{\dot{y_0}^2} \quad \eta_2 = \frac{l}{z_0} \quad \eta_3 = \frac{x_0}{z_0}$$

so we will have

$$\theta_{\text{prec}} = F(\eta_1, \eta_2, \eta_3)$$

where F is an unknown function to be determined. For the sake of further research we will assume it is of the form:

$$\theta_{\text{prec}} = \Gamma \eta_1^\alpha \eta_2^\beta \eta_3^\gamma$$

where all $\Gamma, \alpha, \beta, \gamma$ are constants to be determined. To determine them, η_i will be varied for all i and general linear regressions will be performed to obtain the coefficients. In particular we will perform a regression of the form,

$$\log \theta = \log \Gamma + \alpha \log \eta_1 + \beta \log \eta_2 + \gamma \log \eta_3$$

We can construct some exploratory plots to check qualitatively if our assumptions make sense. These are available in Figure 5 where we can see some promising relationships in the "loglog" plots. We can now perform multiple regression, using the `Python` package `sklearn` (14) and its class `LinearRegression`. The results from the regression are available in Table 1.

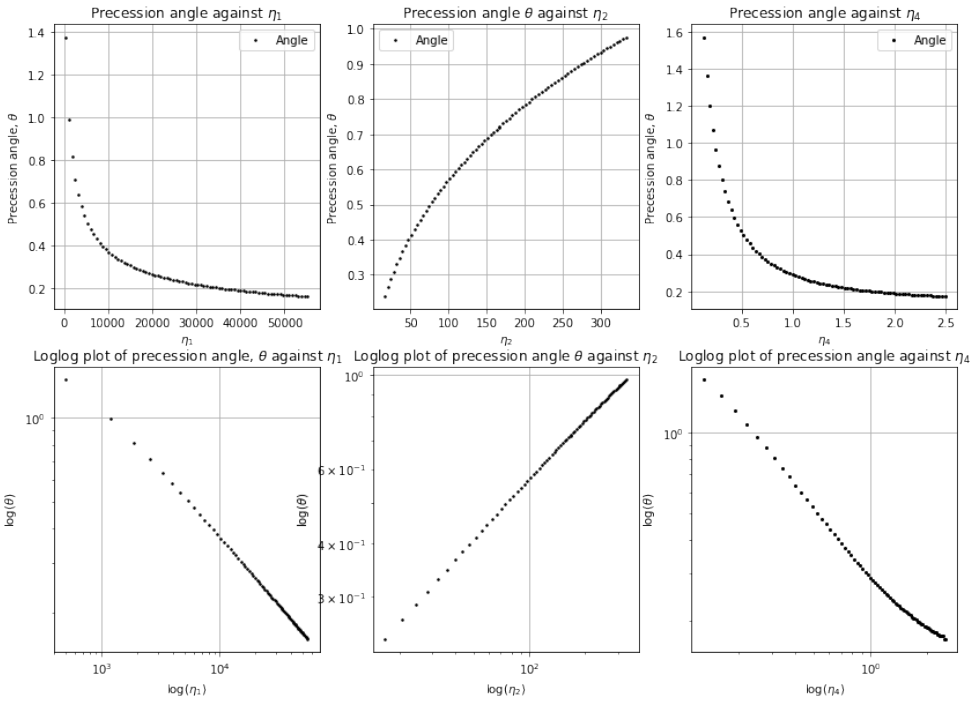

Figure 5: Regressions for the precession angle

Variables	Slope	Range of values
η_1	$\alpha = -0.48866702$	$g \in (2.5, 110)$
η_2	$\beta = 0.4974448$	$l \in (0.4, 1.2)$
η_3	$\gamma = -0.85726894$	$x_0 \in (0.002, 0.03)$
Intercept	$\Gamma = 2.0960532442237$	

Table 1: Regression estimators for the dimensionless groups.

Furthermore the adjusted R^2 coefficient was found to be 0.9971274, very close to 1, suggesting the intuition from Figure 5 has good founding. The closeness in absolute value between α and β suggests we can approximate $\alpha = -\beta$, and thus

$$\theta_{\text{prec}} = \Gamma \left(\frac{l y_0}{g z_0^2} \right)^{\beta} \left(\frac{x_0}{z_0} \right)^{\gamma}$$

These numerical values suggest a possible further approximation to

$$\alpha = -0.5 \quad \beta = 0.5 \quad \Gamma = 2$$

which in turn induces the formula

$$\theta_{\text{prec}} \approx 2\frac{\dot{y_0}}{\sqrt{gz_0}}\sqrt{\frac{l}{z_0}}\left(\frac{x_0}{z_0}\right)^{\gamma} = 2\frac{\dot{y_0}}{z_0}\sqrt{\frac{l}{g}}\left(\frac{x_0}{z_0}\right)^{\gamma}$$

As a mathematical remark, $|\gamma| \approx \tan\left(\frac{1}{\sqrt{2}}\right)$

4.1 Evaluation of the stepwise precession scaling formula via its applications

In this section we will explore the accuracy of our scaling approximation by asking the formula what values of x_0 should we use to get certain precession angles (i.e. solving for x_0 in the approximation). We will choose only angles of the form $\frac{\pi}{n}$ with $n \in \{2, 3, 4, 5, 6, 7, 8, 9\}$, plotted as $2n$ pointed "stars" formed by the horizontal projection onto the $x - y$ plane.The results for this are arrayed in Figure 6. Moreover, the error

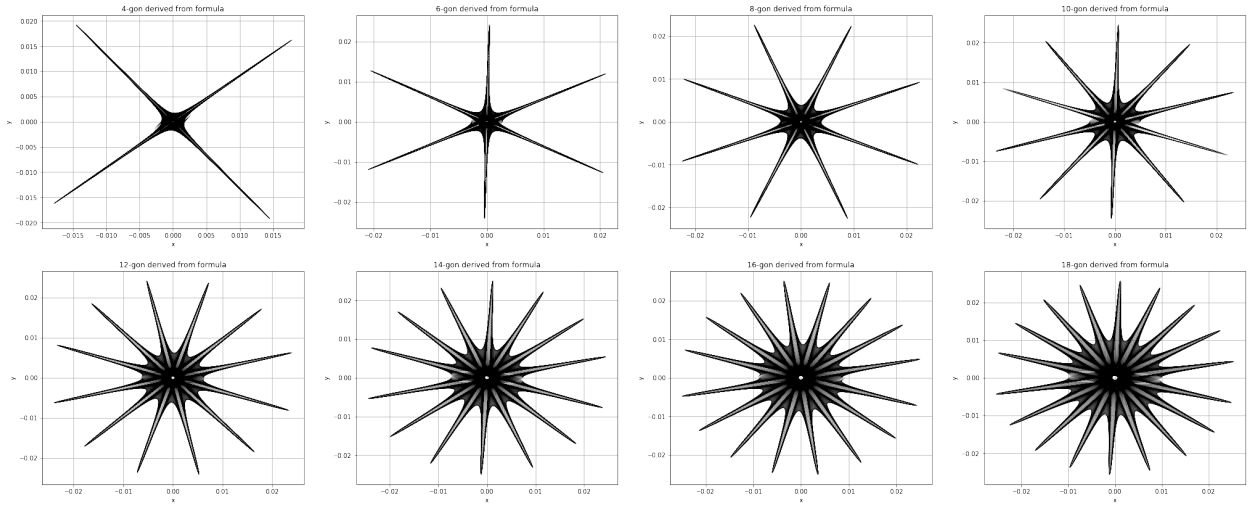

Figure 6: Evaluation of the formula by regular n-star generation

in the precession angle for each of the above figures was computed. This is displayed in Figure 7 alongside a plot of the function $x_0(\theta_{\text{prec}})$, x_0 as a function of the precession angle.

It is evident (from the stars as well) that the error for large angles is significantly larger. This is mainly for two reasons. First, in the formula we see that there's asymptotic behaviour around $x_0 = 0$. This is because it is not possible to get a precession angle of 180^{o}. This in turn induces a singularity in the formula which means that when x_0 is close to 0 a small change in x_0 induces a large change in the precession angle. This might be a reason for the failure of the regression around this area. Secondly, the value of x_0 required for the $\frac{\pi}{2}$ angle outside of the domain of values used in the regression, and it is being effectively extrapolating

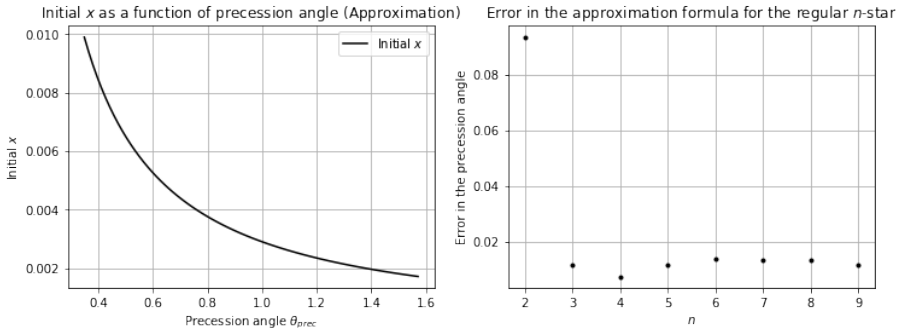

Figure 7: Right: error in the Precession angle for the stars in Figure 6. Left: a plot of $x_0(\theta_{\text{prec}})$

it. This means we are more uncertain about the behaviour around this area. Moreover, we can see some of the figures match almost exactly what is expected, namely for 8, 12 and 16 vertices.

5 Behaviour of 1:1:2 resonant system in a rotating frame

5.1 Spring Foucault's pendulum with 1:1:2 resonance

So far, we have considered a system in an inertial frame of reference, i.e. a frame of reference that is not undergoing acceleration. Therefore, in this section we assess the behaviour of the spring pendulum, with 1:1:2 resonance, within a rotating frame, that could be represented for instance by Earth's rotation. Similarly to the well-known Foucault's pendulum (15) (where, though, the elasticity of the metal rod was neglected), we introduce a rotation term in the Hamiltonian and Lagrangian, i.e. a function of phase space that generates rotation (16, 17):

$$H_{\text{Rot}} = H_{112} + 2\Omega_z J \qquad\qquad L_{\text{Rot}} = L_{112} + 2\Omega_z J$$

where Ω_z is the rotation rate around the z-axis (angular velocity) and J is the angular momentum with respect to the z-axis. It is now important to notice that H_{Rot} preserves the Hamiltonian property of the commutation of Poisson brackets; also, energy is conserved (this is a result of the fact that J is a constant of motion). Euler-Lagrange equations become:

$$\ddot{x} + \omega_R^2 x - 2\Omega_z \dot{y} = \lambda x z$$

$$\ddot{y} + \omega_R^2 y + 2\Omega_z \dot{x} = \lambda y z$$

$$\ddot{z} + \omega_Z^2 z = \frac{1}{2}\lambda(x^2 + y^2)$$

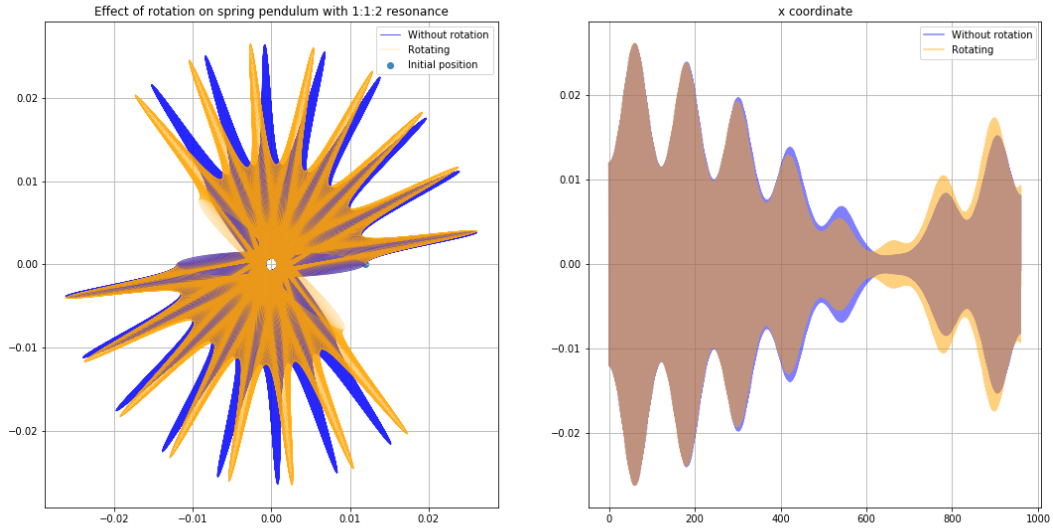

Figure 8: Stepwise precession is conserved in spring Foucault's pendulum with 1:1:2 resonance

We have simulated these equations of motion and compared to the ones without a rotation term. Parameters and initial conditions are tuned to be: $\Omega_z \approx 7.292116 \cdot 10^{-5}$ rad/s, which is Earth's angular velocity, and the others as in *Section 3.3*. From this simulation (see Figure 8) we can infer that stepwise precession is conserved. Yet, it is visibly affected by the effect of the rotation of the Earth. The precession angle is still constant but it is slightly bigger as a result of the constant angular velocity of the rotation frame. Measuring the difference we get $\Delta\theta_{\text{measured}} \approx 0.01199$ rad, which is consistent with the result $\Delta\theta_{\text{theory}} = (\Omega_z \text{ rad/sec})(T \text{ sec}) \approx 0.01196$ rad where T is the time the pendulum takes to complete a stepwise precession ($T \approx 164$ sec).

5.2 Stochastic Analysis

The main purpose of this section is to conduct a stochastic analysis on the precession property of our 1:1:2 system adding a stochastic noise to the angular momentum (which is a constant of motion (1)). This differs from the previous analysis as the noise induced to the angular momentum is stochastic and may comprehend Earth's rotation but also other factors that can be found in nature. As a result of the numerous factors that can affect the studied system, we believe a stochastic analysis to be appropriate.

We begin this section by noting that the Hamiltonian for the 1:1:2 resonance is:

$$H_{112} = \frac{1}{2m}(p_x^2 + p_y^2 + p_z^2) + \frac{m}{2}(\omega_R^2(x^2 + y^2) + \omega_Z^2 z^2) - \frac{m\lambda z}{2}(x^2 + y^2)$$

Furthermore the angular momentum around the z-axis is (1):

$$J = x\dot{y} - y\dot{x} = \frac{1}{m}(xp_y - yp_x)$$

We introduce the following stochastic process, where the stochasticity goes into a Stratonovich semimartinagle Hamiltonian given by

$$dh = H_{112}dt + \sigma J \circ dW_t \tag{5.1}$$

with dW_t a standard Wiener process, $\circ$ represents the Stratonovich Integral and σ is a scaling factor (time-independent) that allows us to scale the magnitude of the noise induced on the angular momentum.

Once again, it is important to highlight that the system with the noise considered in (5.1) is Hamiltonian, i.e. Poisson brackets commute, even though total energy is not conserved as Brownian motion is time dependent. The reason behind this relies in the nature of Stratonovich semimartingales, but a rigorous treatment is beyond the scope of the report and can be found in (18).

The stochastic equations of motion in Hamiltonian form ($H = H_{112}$) are then obtained by applying Poisson brackets:

$$dx_i = \frac{\partial dh}{\partial p_{x_i}} = \frac{\partial H}{\partial p_{x_i}}dt + \sigma\frac{\partial J}{\partial p_{x_i}} \circ dW_t$$

$$dp_{x_i} = -\frac{\partial dh}{\partial x_i} = -\frac{\partial H}{\partial x_i}dt - \sigma\frac{\partial J}{\partial x_i} \circ dW_t$$

For the sake of the numerical simulation, we transform the above SDEs into Îto form by the following formula from (19)

$$d\mathbf{x} = \mathbf{f}(\mathbf{x}, t)dt + \mathbf{L}(\mathbf{x}, t) \circ dW_t \quad \text{into} \quad d\mathbf{x} = \tilde{\mathbf{f}}(\mathbf{x}, t)dt + \mathbf{L}(\mathbf{x}, t)dW_t$$

with

$$\tilde{f}_i(\mathbf{x}, t) = f_i(\mathbf{x}, t) + \frac{1}{2}\sum_{j,k}\frac{\partial L_{ij}}{\partial x_k}L_{kj}$$

In our case $\tilde{f}_i(x, t) = f_i(x, t)$, taking as the vector $\mathbf{x} = (x, y, z, p_x, p_y, p_z)^T$

$$\mathbf{f} = \left(\frac{p_x}{m}, \frac{p_y}{m}, \frac{p_z}{m}, -mx(\omega_R^2 - \lambda z), -my(\omega_R^2 - \lambda z), -m(w_Z^2 z - \frac{1}{2}\lambda(x^2 + y^2)\right)^T$$

$$L = \sigma \text{ diag}\left(\frac{-y}{m}, \frac{x}{m}, 0, \frac{-p_y}{m}, \frac{p_x}{m}, 0\right)$$

where diag denotes a diagonal matrix. Then it is easy to verify that $\tilde{f}_i(x,t) = f_i(x,t)$ for all i and now that our SDE is in Îto form we can integrate it using the explicit Euler-Maruyama procedure. However, this scheme depends on $\sqrt{\Delta t}$, which means we will need many timesteps to integrate it. For this reason a Range-Kutta like scheme is introduced to avoid excessive computation time (20). Other possible integration schemes are avialable in (21, 22)

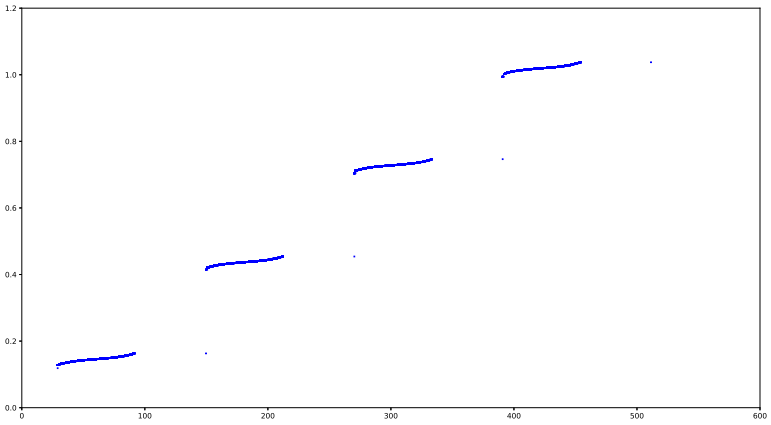

Figure 9: Angle between the swing plane and x-axis over time. Blue dot placed every time pendulum was far away from the origin. Lines correspond to periods of swinging motion, gaps correspond to periods when swinging was weak.

As it can be observed in Figure 6 the motion of spring pendulum is a combination of swinging and vertical motion. During some periods the swinging dominates and the pendulum regularly moves far away from the origin. When the swinging decreases, vertical motion prevails and the pendulum stays close to the origin. In Figure 9 we plotted a blue dot every time pendulum moved far away from the origin (i.e. when the swinging motion was strong). There were extended periods of time when no blue dot was plotted, corresponding to the periods when swinging was weak and pendulum stayed close to the origin. Each blue line on the diagram corresponds to the angle swing plane makes with x-axis during a given period. One can see that this angle stays constant for some time and then, after a period of weak swinging motion (seen as gaps between blue lines), increases. These increases are constant in time.

Precession persists even under the influence of stochastic effects. As can be seen in the figures below (Figure 10), the noise makes the trajectory more dispersed, but the precession is still present. While precession persists under the influence of stochastic effects, the noise makes the precession occur at increasingly shorter intervals as time increases (Figure 12). Figures 11 and 12 were constructed in a similar manner as Figure 9.

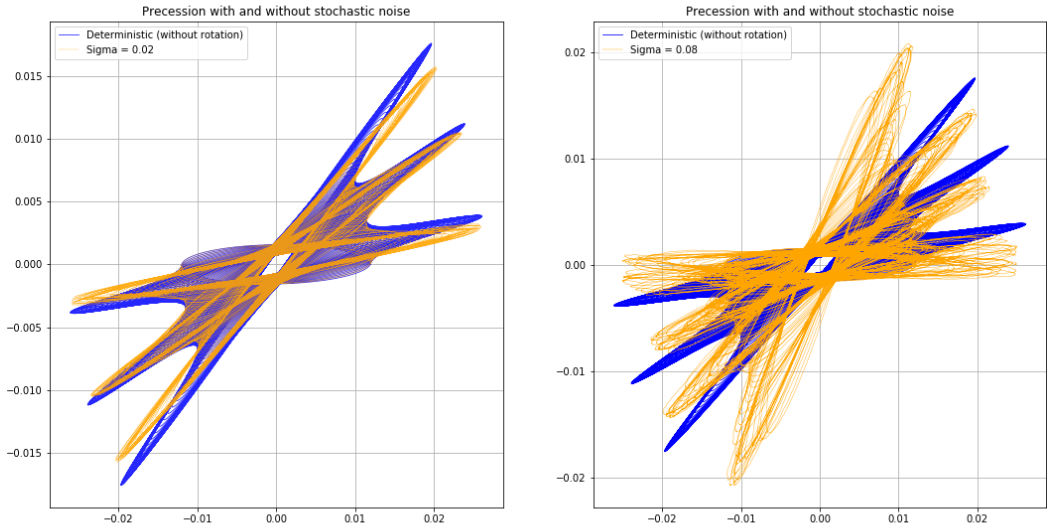

Figure 10: Spring pendulum with 1:2:2 resonance and induced-random noise. Stepwise precession is conserved.

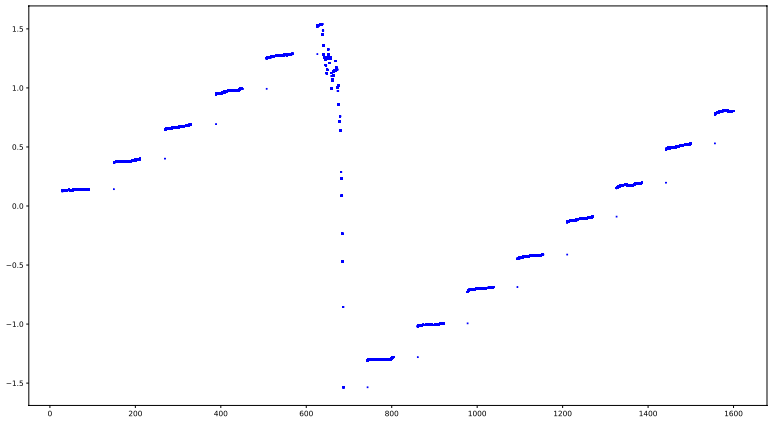

Figure 11: Angle between the swing plane and x-axis over time with $\sigma = 0.01$. Blue dot placed every time pendulum is 0.018 m from the origin. Lines correspond to periods of swinging motion, gaps correspond to periods when swinging is weak and vertical motion prevails.

Acceleration of precession rate scales with the magnitude of σ, which is why for small values of σ precession seems to happen at constant intervals (Figure 11), but for larger values one can clearly see that the precession

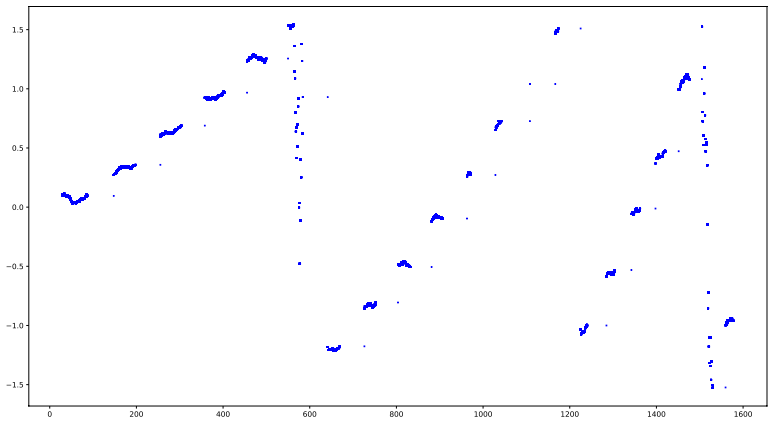

Figure 12: Angle between the swing plane and x-axis over time with $\sigma = 0.04$. Blue dot placed every time pendulum is 0.018 m from the origin. Lines correspond to periods of swinging motion, gaps correspond to periods when swinging is weak and vertical motion prevails.

is happening at an accelerating rate (Figure 12). This is observed by the consistent increase in gradients and decrease of lengths of the blue lines, meaning that the time pendulum spends in swinging motion decreases with time.

5.3 Conclusion and the connection to Monodromy

Monodromy can be traced back to the phrase "running round singly", which offers a more generalised definition to the notion. Instead of the focus on ramification (branch) points, we look at monodromy as the measure of the behaviour of a system, as it encirlces a singularity (23). A definition which clarifies monodromies' existence in the Foucault pendulum. As observed in Figure 8, both the regular and Foucault spring pendulums orbit the central (singular) point, $\Upsilon = (0, 0, 0)$. This shared singularity, Υ, topologically displaces the sphere after each complete revolution of a Υ-centred monodromy circuit, i.e. the swings of the pendulum (10).

The main result of our analysis is that inducing rotation (with respect to the z-axis) to the system, does not change the nature of the singularity of the origin $(0, 0, 0)$, which is invariant under rotation and gravity. In fact, at this singular point, the azimuthal angle of the pendulum is always undefined (with respect to our coordinate system). This leads to the monodromy which is responsible for the stepwise precession observed both in the initial and rotation-induced systems (1).

When it comes to the stochastic analysis, once again we observe that for sufficiently small σ (as energy is not conserved due to the effect of the introduction of Brownian motion), the singularity at $(0,0,0)$ is preserved thus leading to stepwise precession. Yet, if in the deterministic rotation the precession angle was constant, in the stochastic setting we observe that precession occurs at an accelerated rate.

6 The 1:2:2 resonance

Consider system with potential

$$\frac{1}{2}(x^2+4y^2+4z^2)-x^2(a_1y+a_2z),$$

with constant coefficients a_1, a_2. Noting that kinetic energy of mass m is $E_k = \frac{m}{2}\left(\dot{x}^2+\dot{y}^2+\dot{z}^2\right)$ and assuming $m=1$ we get cubic Lagrangian

$$L_{122} = \frac{1}{2}(\dot{x}^2+\dot{y}^2+\dot{z}^2)-\frac{1}{2}(x^2+4y^2+4z^2)+x^2(a_1y+a_2z).$$

Using Euler-Lagrange equations (2) for this system we get the following equations of motion:

$$\begin{aligned}
\ddot{x} \;+\; x &= 2x(a_1y+a_2z)\\
\ddot{y} \;+\; 4y &= a_1x^2\\
\ddot{z} \;+\; 4z &= a_2x^2
\end{aligned}$$

6.1 A brief discussion of the equilibrium behaviour

We can see from the system that equilibrium points (in $\mathbb{R}^6$) must satisfy:

$$\dot{x}=\dot{y}=\dot{z}=0 \qquad y=\frac{a_1x^2}{4} \quad z=\frac{a_2x^2}{4}$$

$$x=0 \quad \text{or} \quad 2a_1y+2a_2z=1$$

Choosing $x=0$ we just get the trivial equilibrium $\mathbf{0}\in\mathbb{R}^6$. Furthermore, this equilibrium point is non hyperbolic, as all the eigenvalues of the linearisation are purely imaginary (i.e. the real part is zero), so no useful information on its stability can be inferred from linearisation. However it can be verified numerically that the equilibrium is in fact unstable. Choosing the non trivial condition and substituting y and z, we get

that

$$1 = \frac{x^2}{2}(a_1^2 + a_2^2) \Longrightarrow x = \pm\sqrt{\frac{2}{a_1^2 + a_2^2}}$$

and thus for this equilibrium point,

$$y = \frac{a_2}{2(a_1^2 + a_2^2)} \quad z = \frac{a_1}{2(a_1^2 + a_2^2)}$$

As we will see in the upcoming sections, numerical results suggest these equilibria are also unstable as small perturbations of the equilibria get further away from them.

Proposition 6.1. ***Invariant sets*** *If* $a_2 y_0 - a_1 z_0 = a_2 \dot{y} - a_1 \dot{z}_0 = 0$ *then the plane* $a_2 y = a_1 z$ *is positively invariant (9).*

Proof. Define $\xi := a_2 y - a_1 z$. Note that from the bottom two equations

$$x^2 = \frac{\ddot{y} + 4y}{a_1} = \frac{\ddot{z} + 4z}{a_2}$$

and we can rearrange the latter equality

$$\frac{\ddot{y}}{a_1} - \frac{\ddot{z}}{a_2} = 4\left(\frac{y}{a_1} - \frac{z}{a_2}\right) \Longrightarrow \ddot{\xi} = -4\xi$$

we can solve that ODE for ξ

$$\xi(t) = C_1 \sin(4t) + C_2 \cos(4t)$$

Now, using the initial conditions that $\xi(0) = \dot{\xi}(0) = 0$ both $C_1 = C_2 = 0$ and thus $\xi(t) = 0 = a_2 y(t) - a_1 z(t)$ as required, proving that the aforementioned plane is positively invariant. Moreover, this solution gives us more information on the system even when we start outside the set in the question. It tells us we will oscillate around the plane but never get too far away. Of course this plane is infinite so this does not mean the motion can not diverge (i.e. x still can be unbounded).

6.2 Average Lagrangian and average Euler-Lagrange equations

Using the same approach as for 1:1:2 (see *section 3.1* and (1, 4)), adapted for the new resonance ratios, we define:

$$x = \Re[a(t)\exp(i\omega t)] \quad y = \Re[b(t)\exp(2i\omega t)] \quad z = \Re[c(t)\exp(2i\omega t)]$$

Now, plugging these into L_{122}/m, the terms with a complex exponential factor are neglected as they will integrate to zero when calculating the action, and furthermore, non-dimensionalising the problem so that $\omega = 1$, we get:

$$\langle L \rangle = \frac{\Im[\dot{a}a^* + 2\dot{b}b^* + 2\dot{c}c^*]}{2} + \frac{\Re[a^2(a_1 b^* + a_2 c^*)]}{4}$$

Please, see *Appendix* for full calculations. From the average Lagrangian, which can be expanded as follows

$$\langle L \rangle = \frac{\dot{a}a^* - \dot{a}^* a + 2(\dot{b}b^* - \dot{b}^* b) + 2(\dot{c}c^* - \dot{c}^* c)}{4i} + \frac{(a^2(a_1 b^* + a_2 c^*) + (a^*)^2(a_1 b + a_2 c)}{8}$$

we can derive the averaged Euler-Lagrange equations:

$$\frac{\partial \langle L \rangle}{\partial a^*} = \frac{\dot{a}}{4i} + \frac{a_1 a^* b + a_2 a^* c}{4} \qquad \frac{\partial \langle L \rangle}{\partial \dot{a}^*} = \frac{-a}{4i}$$

And

$$\frac{d}{dt}\left(\frac{\partial \langle L \rangle}{\partial \dot{a}^*}\right) = \frac{\partial \langle L \rangle}{\partial a^*} \implies -\frac{\dot{a}}{4i} = \frac{a_1 a^* b + a_2 a^* c}{4} + \frac{\dot{a}}{4i} \implies -\frac{\dot{a}}{2i} = \frac{a_1 a^* b + a_2 a^* c}{4}$$

leading to:

$$i\dot{a} = \frac{a^*}{2}(a_1 b + a_2 c)$$

Proceeding similarly for b,

$$\frac{\partial \langle L \rangle}{\partial b^*} = \frac{a_1 a^2}{8} + \frac{\dot{b}}{2i} \qquad \frac{\partial \langle L \rangle}{\partial \dot{b}^*} = -\frac{b}{2i}$$

Combining them as previously:

$$-\frac{\dot{b}}{2i} = \frac{a_1 a^2}{8} + \frac{\dot{b}^*}{2i} \implies -i\dot{b} = i^2 \frac{a_1 a^2}{8} \implies i\dot{b} = \frac{a_1 a^2}{8}$$

Using a symmetry argument the E-L equation for c can be readily inferred,

$$i\dot{c} = \frac{a_2 a^2}{8}$$

Summarizing, we have:

$$i\dot{a} = \frac{a^*}{2}(a_1 b + a_2 c) \qquad i\dot{b} = \frac{a_1 a^2}{8} \qquad i\dot{c} = \frac{a_2 a^2}{8}$$

6.3 Three-wave interaction equations for complex amplitude of 1:2:2 resonance

Let us consider the following transformation:

$$A = \frac{1}{\sqrt{2}}a \qquad B = b \qquad C = c$$

Implying

$$i\dot{A} = \frac{1}{\sqrt{2}}i\dot{a} = \frac{1}{\sqrt{2}}\frac{a^*}{2}(a_1 b + a_2 c) = \frac{A^*}{2}(a_1 B + a_2 C)$$

$$i\dot{B} = i\dot{b} = \frac{a_1 a^2}{8} = \frac{a_1 A^2}{4} \qquad i\dot{C} = i\dot{c} = \frac{a_2 a^2}{8} = \frac{a_2 A^2}{4}$$

The three-wave interaction equations may be written in canonical form with Hamiltonian

$$H = \frac{1}{4}\Re[A^2(a_1 B^* + a_2 C^*)]$$

and Poisson brackets $\{A, A^*\} = \{B, B^*\} = \{C, C^*\} = -2i$ that give us

$$i\dot{A} = i\{A, H\} = 2\partial H/\partial A^*$$

$$i\dot{B} = i\{B, H\} = 2\partial H/\partial B^*$$

$$i\dot{C} = i\{C, H\} = 2\partial H/\partial C^*$$

6.4 Integrability

An important notion to explore next, is the integrability of our two different 3-mode systems of resonant oscillators. While it is well known that the 1:1:2 comprises of a completely integrable Hamiltonian system, we build on our understanding for the 1:2:2 case by finding constants of motion.

6.4.1 Constants of motion

Consider the following mapping:

$$N : \begin{pmatrix} a \\ b \\ c \end{pmatrix} \rightarrow \begin{pmatrix} ae^{i\epsilon} \\ be^{2i\epsilon} \\ ce^{2i\epsilon} \end{pmatrix}$$

The Lagrangian is invariant under this mapping, hence by Noether's theorem (2) we can find a constant of motion.

Linearisation of N yields

$$\begin{pmatrix} a \\ b \\ c \end{pmatrix} \rightarrow \begin{pmatrix} a + \epsilon \frac{d}{d\epsilon} \left(a e^{i\epsilon} \right) |_{\epsilon=0} \\ b + \epsilon \frac{d}{d\epsilon} \left(b e^{2i\epsilon} \right) |_{\epsilon=0} \\ c + \epsilon \frac{d}{d\epsilon} \left(c e^{2i\epsilon} \right) |_{\epsilon=0} \end{pmatrix} = \begin{pmatrix} a + K_a \epsilon \\ b + K_b \epsilon \\ c + K_c \epsilon \end{pmatrix}, \qquad \text{with } K_a = ia,\ K_b = 2ib,\ K_c = 2ic$$

From Noether's Theorem (2) we have that

$$\frac{\partial L}{\partial \dot{a}} K_a + \frac{\partial L}{\partial \dot{b}} K_b + \frac{\partial L}{\partial \dot{c}} K_c$$

is conserved. Substituting vales of K_a, K_b, K_c and partial derivatives we obtain

$$\frac{\partial L}{\partial \dot{a}} ia + \frac{\partial L}{\partial \dot{b}} 2ib + \frac{\partial L}{\partial \dot{c}} 2ic \ = \ \left(-\frac{1}{4} ia^* \right) ia + \left(-\frac{1}{2} ib^* \right) 2ib + \left(-\frac{1}{2} ic^* \right) 2ic \ = \ \text{const.}$$

$$\implies \quad \frac{1}{4} |a|^2 + |b|^2 + |c|^2 \ = \ \text{const.}$$

This constant of motion in terms of our new variables A, B, C reads as

$$|A|^2 + 2|B|^2 + 2|C|^2 = \ \text{const.}$$

In addition to the above constant of motion, we obtain further constants from the Euler-Lagrange equations, alongside the realisation that:

$$i \frac{d}{dt} \left(a_2 B - a_1 C \right) = a_2 i \dot{B} - a_1 i \dot{C} = \frac{a^2}{4} \left(a_1 a_2 - a_1 a_2 \right) = 0$$

$$\implies a_2 B - a_1 C = \ \text{const.}$$

thus implying that both the real and the imaginary part of $a_2 B - a_1 C$ are constant.

6.4.2 Integrability for the 1:2:2 resonance

To summarize, our three (transformed) non-Hamiltonian constants of motion: $\{C_J, H_{122}\} = 0,\ J = 0, 1, 2$ read as

$$\begin{aligned} C_0 &= |A|^2 + 2|B|^2 + 2|C|^2 \\ C_1 &= a_2\Re(B) - a_1\Re(C) \\ C_2 &= a_2\Im(B) - a_1\Im(C) \end{aligned} \tag{6.1}$$

For integrability, we require the constants of motion to Poisson-commute both with H_{122}, and amongst themselves. Sadly, this is not satisfied in the 1:2:2 case

$$\{C_1, C_2\} = -a_1^2 - a_2^2 \neq 0 \tag{6.2}$$

7 An Approximation for 1:2:2

Gaining insights from a non-integrable system is often a difficult process, yielding limited results on interesting topics such as Chaos. In this section we tackle this by building a good (integrable) approximation to our Hamiltonian, and applying it in various ways.

7.1 A New Hamiltonian

In (24), a unique and integrable general three dof Hamiltonian normal form (in first order resonance) was shown to exist. Its form, as shown below, allows the original Hamiltonian, H_{122}, to behave as an integrable system with error $O(\epsilon)$ on the timescale $\frac{1}{\epsilon}$.

$$H_2 = \frac{1}{2}(x^2 + p_x^2) + \frac{1}{2}(4y^2 + p_y^2) + \frac{1}{2}(4z^2 + p_z^2)$$

$$\bar{H}_3 = 2a_1\{y(x^2 - p_x^2) + xp_xp_y\} + a_2\{p_y(p_x^2 - x^2) + 4xyp_x\} + 2a_3\{z(x^2 - p_x^2) + xp_xp_z\}$$

$$+a_4\{p_z(p_x^2 - x^2) + 4xzp_x\}$$

$$\bar{H} = H_2 + \epsilon\bar{H}_3$$

Where a_1, a_2, a_3, a_4 are constants and the Hamiltonian, H, is expressed in coordinates $q(x, y, z)$ and the corresponding momenta $p(p_x, p_y, p_z)$.

In fact, Van Der & Verhulst's "Particular Potential Problem" (24) shares a striking similarity to our system, allowing us to easily tailor the above generalised form to our system. This gives:

$$\bar{H}_{122} = H_2 - \frac{1}{4}[a_1\{y(x^2 - p_x^2) + xp_xp_y\} + a_2\{z(x^2 - p_x^2) + xp_xp_z\}]$$

where in our system, $p_x = \dot{x}$, $p_y = \dot{y}$ and so on.

7.2 Chaos

Often, to explore chaos in non-integrable systems, we start by outlining a suitable approximation to the system (25). Here a "suitable" approximation is an integrable Hamiltonian with a sensible error. Doing this provides a good error estimate for H_{122}, permitting us to measure local regularity and chaos.

7.2.1 Stability Analysis for a Normal Mode

As the analysis of systems in (24) has shown, we are able to learn more about the stability of our normal modes. Using a similar implementation, we analyse here the stability of the normal mode in the y-direction for our $\bar{H}_{122}$, whose existence is confirmed in (26).

Our normal mode in the y-direction is found by plugging $x = \dot{x} = z = \dot{z} = 0$ into our 1:2:2 system of equations resulting in a harmonic solution in y from $\ddot{y} + 4y = 0$. Defining:

$$q_1 = x, \qquad p_1 = p_x, \qquad q_3 = \sqrt{2}z, \qquad p_3 = \frac{p_z}{\sqrt{2}},$$

while using action-angle coordinates in the plane (r_2, ϕ_2), $\bar{H}_{122}$ becomes:

$$\bar{H}_{122} = \frac{1}{2}(q_1^2+p_1^2)+2r_2+(q_3^2+p_3^2)-\frac{1}{8}[2a_1\sqrt{r_2}\{(q_1^2-p_1^2)\sin\phi_2+2q_1p_1\cos\phi_2\}+a_2\sqrt{r_2}\{q_3(q_1^2-p_1^2)+2q_1p_1p_3].$$

As in (24), we then define $\mathcal{H} = \bar{H}_{122} - H_2$, utilise the Lagrange-multipliers method and see our normal mode is given by $q_1 = p_1 = q_3 = p_3 = 0, H_2 = E \ \ \& \ \ r_2 = \frac{1}{2}E$. Considering the eigenvalues for the matrix:

$$d^2\mathcal{H} = \begin{bmatrix} -\frac{1}{2}a_1\sqrt{r_2}\sin\phi_2 & -\frac{1}{2}a_1\sqrt{r_2}\cos\phi_2 & 0 & 0 \\ -\frac{1}{2}a_1\sqrt{r_2}\cos\phi_2 & \frac{1}{2}a_1\sqrt{r_2}\sin\phi_2 & 0 & 0 \\ 0 & 0 & 0 & 0 \\ 0 & 0 & 0 & 0 \end{bmatrix}$$

we get: $\lambda_1 = \lambda_2 = 0$, $\lambda_3 = \frac{1}{2\sqrt{2}}a_1\sqrt{E}$ & $\lambda_4 = -\frac{1}{2\sqrt{2}}a_1\sqrt{E}$.

Thus, $\forall a_1 \neq 0$, we always have one positive eigenvalue, meaning this normal mode is unstable (27). And in the case where $a_1 = 0$, we also have instability due to the presence of 0 eigen-values (28). This of course implies instability of the flows near the normal mode, as illustrated in (24).

7.2.2 Conclusion

In the above analysis, flows near the normal mode were shown to be unstable, but what does that mean? Unstable trajectories starting in close proximity will at some point in time, diverge exponentially. In dynamical systems, the instability of trajectories acts as a criteria for chaotic behaviour (29) which is commonly observed in non-integrable Hamiltonian systems. In fact, to prove the existence of chaos, we additionally require the global confinement of trajectories in the phase space (30). Given existence, a systems' high sensitivity to intial conditions is established, as seen in Figure 4.

7.3 Numerical results for the 1:2:2 resonance and evaluation of the SVE approximation

The aim of the present section is to numerically explore the behaviour of the solutions when the equilibria are perturbed and evaluate the SVE approximation for the 1:2:2 resonance. As for the 1:1:2 resonance, the equations were integrated with `SciPy`'s (6) built in ODE solver. The SVE equations are expanded into real and imaginary parts to form 6 real ODEs. The initial conditions are computed as in the 1:1:2 case but with $\omega_R = 1$ and furthermore frequency terms in y are twice than what they were in 1:1:2, accounting for the new resonance. First and foremost, it is observed that the SVE approximation only works for small values of a_1 and a_2. This is intuitive as in the approximation of the average Lagrangian terms with derivatives

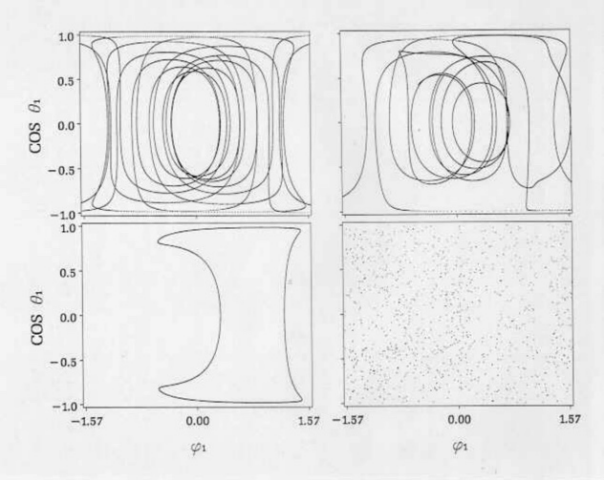

Figure 13: Phase-space trajectories (Top) and Poincare maps (Bottom) for a non-integrable system with sensitive dependence on initial conditions. Clear distinction between regular (left) and chaotic (right) trajectories. (Diagram obtained from (31))

squared (of the form $\frac{da}{dt}\frac{da^*}{dt}$) were neglected as the envelopes are assumed to vary slowly. However, as the derivative of both b and c are proportional to a_1 and a_2 respectively, when these values are not small the approximation inevitably will fail, as the derivatives are not small either. This can be seen for instance by taking $a_1 = a_2 = 1$ and setting some initial conditions close to one of the non-trivial equilibria, say $(1, \frac{1}{4}, \frac{1}{4})$, shown in Figure 14.

In Figure 14 we can see the error for the SVE equations is sometimes twice as large as the actual value, a relative error of around 200%, suggesting an issue with the SVE approximation. As mentioned above the root cause of this is that some of the derivatives are proportional to the parameters, and hence when the parameters are large so are the derivatives, contradicting the assumption required for the derivation of the approximation. However when we restrict the values of the parameters to, say below 0.1, the SVE approximation is a much better fit. For the sake of clarity only the x coordinate will be shown in Figure 15, where $a_1 = a_2 = 0.01$. Please note the scale for the third plot, as the error is bounded above by 0.014.

As a final figure for the 1:2:2, we can numerically study the stability of one of the non trivial equilibria by simulating the system. The equilibria was perturbed and numerical evidence of chaotic motion was observed, as can be seen in Figure 16a(a), where the projection of the motion onto the $x - y$ plane is shown, as well as the motion in 3D in Figure 16a(b). The initial conditions are $x_0 = 1 - 0.001 \quad y_0 = 0.25 \quad z_0 = 0.24$ and $a_1 = a_2 = 1$, starting from rest.

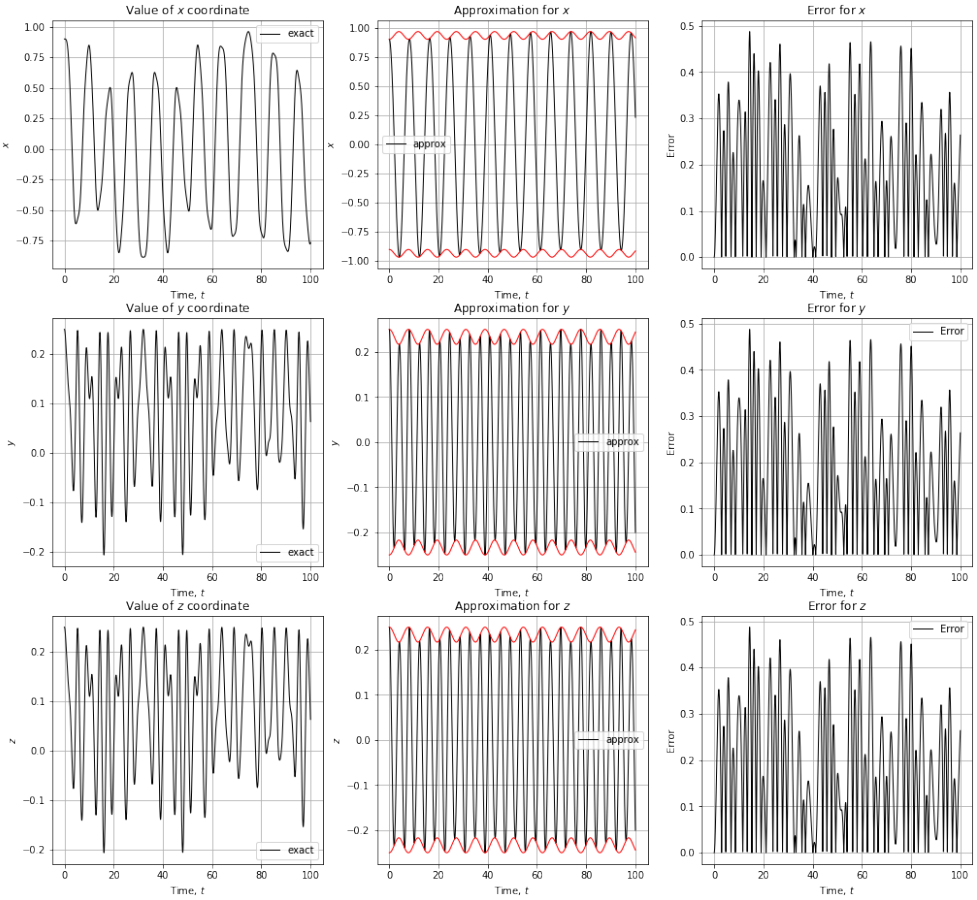

Figure 14: For large values of the parameter the SVE equations fail completely

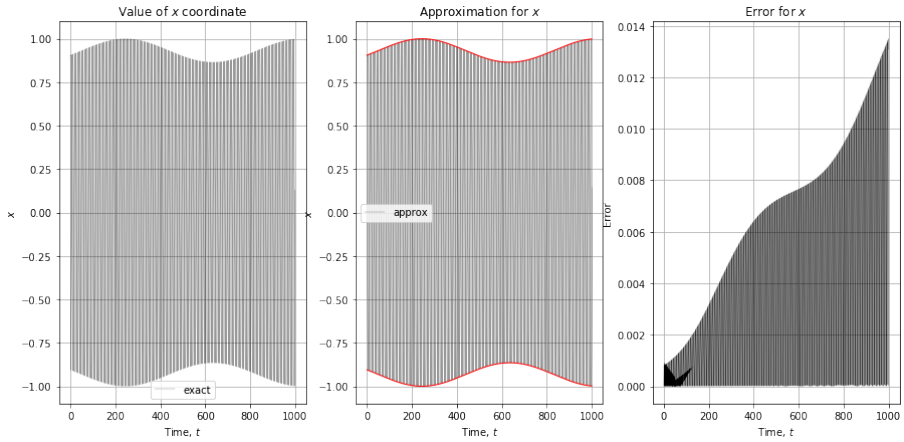

Figure 15: For small values of the parameters SVE equations work excellently

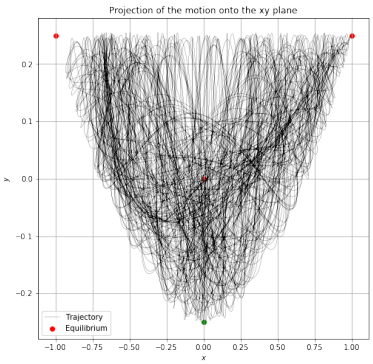

(a) Projection onto the $x - y$ plane

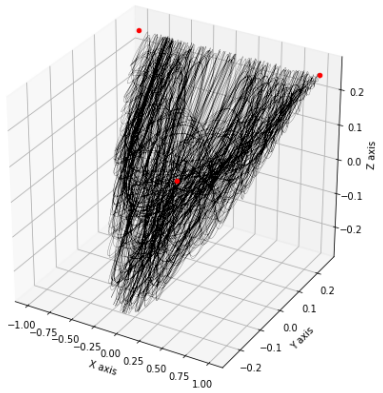

(b) 3D visualisation

Figure 16: Motion for an initial condition of an sightly perturbed equilibrium

7.4 Comparison between 1:1:2 and 1:2:2

After an exhaustive analysis of both systems, it is clear they have very marked differences. Firstly, the 1:1:2 is completely integrable whilst the 1:2:2 is not. This shows that not all dynamical systems are as convenient to work with and exhibit properties as desirable as the elastic spherical pendulum when it is resonating. Moreover the 1:1:2 system displays precession whilst the 1:2:2 does not.

8 Conclusion and applications

We have seen that in the case of the 1:1:2 resonance, approximating the Lagrangian and averaging over the fast times provides us with modulation equations that have three independent constants of motion, and are also integrable.

Our findings have an application to molecular study - something that was first seen with regards to carbon dioxide (CO_2) molecules by Vitt and Gorelik in 1933 (32).
Both optical and electrical data gave us the model of a CO_2 molecule, which can be viewed in Fig. 17a. Via spectral measurements and theoretical conclusions, we know that the CO_2 molecule has ionic oscillations, shown in Fig. 17b, 17c, where the frequency of the first oscillation (the stretching mode) is roughly twice that of the second (the doubly degenerate bending mode) (33). We notice that this is equivalent to the elastic spherical pendulum in 1:1:2 resonance, with the stretching mode representing the springing motion of the pendulum, and the doubly degenerate bending mode representing the swinging.

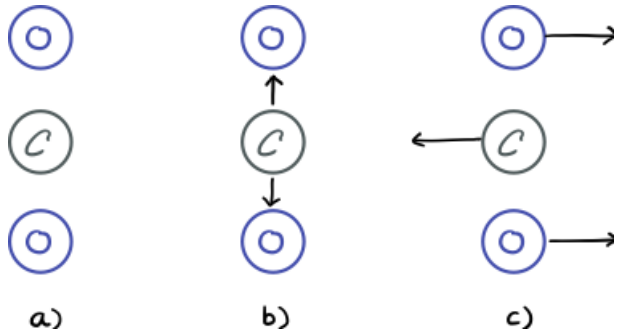

Figure 17: A figure showcasing the Fermi resonance of a CO_2 molecule (Self drawn)

The three-wave equations,

$$i\dot{A} = B^*C \qquad i\dot{B} = A^*C \qquad i\dot{C} = AB$$

can also be used for a variety of other physical applications (4):

- They can be used for modelling the nonlinear dynamics of the amplitudes of three waves in a fluid/plasma (34). They arrive from conducting a perturbation analysis of the barotropic potential vorticity equation:
$$\frac{\partial}{\partial t}\left[\nabla^2\phi - F\phi\right] + \left(\frac{\partial\phi}{\partial x}\frac{\partial\nabla^2\phi}{\partial y} - \frac{\partial\phi}{\partial y}\frac{\partial\nabla^2\phi}{\partial x}\right) + \beta\frac{\partial\phi}{\partial x}$$
- The equations are equivalent to the Maxwell-Schrödinger envelope equations between radiation and a two-level resonant medium in a microwave cavity. (35)
- They also dictate the dynamics of light waves in an inhomogenous material (in the envelope) (36). A geometrical analysis allows the reduced dynamics for these light waves to be depicted as movement on a closed, three-dimensional surface, which is our three-wave surface.
- Under certain conditions, they can be reduced to Euler's equations for a freely rotating rigid body.

Another interesting physical implementation is the Foucault pendulum (see Fig.18) - a (long and heavy) spherical pendulum acting in a rotating frame of reference (e.g. the Earth). Foucault used this pendulum to demonstrate the Earth's rotation, and he observed that this rotation would cause the swing-plane of the pendulum to rotate over time, returning to its original direction after a time period of $T = 24/\sin v_0$ (where v_0 is the latitude at which the experiment occurs on the rotating frame of reference) (15, 37).

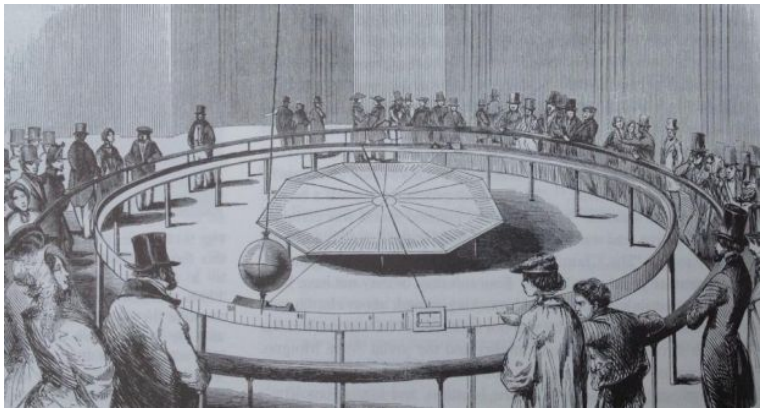

Figure 18: A sketch of a Foucault pendulum as displayed in the Panthéon, Paris, 1851 (Picture obtained from (38))

Even if a metal rod is used for the pendulum, there will still be elasticity present (the degree of which depends on the material in use). If the pendulum is elastic enough and resonance occurs, then a precession angle arises (see Section 4 - and we lose the ability to prove the rotation of the Earth.

References

(1) Holm DD. *Geometric Mechanics Part I: Dynamics and Symmetry,*. 2nd edition. London: World Scientific: Imperial College Press. Available from: `https://www.ma.ic.ac.uk/~dholm/classnotes/GeomMech1-2nd.pdf`. [Accessed 14th June 2021]

(2) Morin D. *Introduction to Classical Mechanics: with Problems and Solutions*. Cambridge: Cambridge University Press; 2007. Print.

(3) Lynch P. Resonant Rossby wave triads and the swinging spring. *Bulletin of the American Meteorological Society*. 2003; 84(5):605–616. Available from: `https://journals.ametsoc.org/view/journals/bams/84/5/bams-84-5-605.xml?tab_body=pdf`. [Accessed 13th June 2021]

(4) Holm DD, Lynch P. Stepwise Precession of the Resonant Swinging Spring.*SIAM journal on applied dynamical systems*. 2002; 1(1)44–64. Available from :`https://epubs.siam.org/doi/pdf/10.1137/S1111111101388571`. [Accessed 4th June 2021]

(5) Whitham GB. *Linear and Nonlinear Waves*. 1974. New York: John Wiley & Sons. Available from: `https://onlinelibrary.wiley.com/doi/book/10.1002/9781118032954`. [Accessed 14th June 2021]

(6) Virtanen P, Gommers R, Oliphant TE, Haberland M, Reddy T, Cournapeau D, et al. SciPy 1.0: Fundamental Algorithms for Scientific Computing in Python. *Nature Methods*. 2020;17:261–72.

(7) Harris CR, Millman KJ, van der Walt SJ, Gommers R, Virtanen P, Cournapeau D, et al. Array programming with NumPy. *Nature*. 2020;585:357–62.

(8) Hairer E, Lubich C, Wanner G. *Geometric Numerical Integration Structure-Preserving Algorithms for Ordinary Differential Equations*. 2nd ed. 2006. Berlin: Springer Berlin Heidelberg, 2006. Available from: `https://link.springer.com/book/10.1007%2F3-540-30666-8`. [Accessed 14th June 2021]

(9) Verhulst F. Henri Poincaré's Neglected Ideas. *Discrete and Continuous Dynamical Systems*. 2020; (Series S) 13(4):1411–2, Available from: `doi:10.3934/dcdss.2020079`.

(10) Salmon D. Dynamics of Systems With Hamiltonian Monodromy. *Dissertations, Theses, and Masters Projects*, 2018, Paper 1550153890.

(11) Cline D. *Action-angle Variables,* University of Rochester, 2021. Available from: `https://phys.libretexts.org/@go/page/9653` [Accessed 11th June 2021]

(12) Wolfram Alpha. *Square Root: 3D Plots Over The Complex Plane,* Available from: `https://functions.wolfram.com/ElementaryFunctions/Sqrt/visualizations/5/`. [Accessed 4th June 2021]. Web.

(13) Sonin AA. *The Physical Basis of Dimensional Analysis*. 2nd Edition. Cambridge: Department of Mechanical Engineering, MIT; 1997. Available from: http://web.mit.edu/2.25/www/pdf/DA_unified.pdf. [Accessed 6th June 2021]

(14) Pedregosa et al. Scikit-learn: Machine Learning in Python. *JMLR*. 2011;12: 2825-2830.

(15) Oprea J. Geometry and the Foucault Problem. *The American Mathematical Monthly*. 2018; 102(6):515-522. Available from: https://www.maa.org/sites/default/files/pdf/upload_library/1/1/Oprea-Ford-1996.pdf. [Accessed 14th June 2021]

(16) Das U, Talukdar B, Shamanna J. Indirect Analytic Representation of Foucault's Pendulum. *Czechoslovak Journal of Physics 52*. 2002; 52:1321–1327. Available from: https://doi.org/10.1023/A:1021819627736.

(17) Rigas I, Sánchez-Soto LL, Klimov AB, **v**Reháv**c**ek J, Hradil Z. Orbital angular momentum in phase space. *Annals of Physics*. 2011; 326(2):429-439. Available from: https://doi.org/10.1016/j.aop.2010.11.016. [Accessed 14th June 2021]

(18) Lázaro-Camí JA, Ortega JP. Stochastic hamiltonian dynamical systems. *Reports on Mathematical Physics*. 2008; 61(1):65-122. Available from: https://doi.org/10.1016/S0034-4877(08)80003-1.

(19) Särkkä S. *Itô Calculus and Stochastic Differential Equations*. [Lecture], Aalto University, Finland (visiting at Oxford University, UK), November 14, 2013. Available from: https://users.aalto.fi/~ssarkka/course_ox2013/pdf/handout2.pdf. [Accessed 14th June 2021]

(20) Roberts AJ. *Modify the Improved Euler scheme to integrate stochastic differential equations,* 2012. Available from: https://arxiv.org/pdf/1210.0933.pdf. [Accessed 14th June 2021]

(21) Rößler A, Runge–Kutta Methods for Stratonovich Stochastic Differential Equation Systems with Commutative Noise, *Journal of Computational and Applied Mathematics* 2004; 164–165:613-627. Available from https://doi.org/10.1016/j.cam.2003.09.009.

(22) Saito Y, Mitsui T. Stability Analysis of Numerical Schemes for Stochastic Differential Equations, *SIAM Journal on Numerical Analysis*. 1996; 33(6):2254-2267. Available from: doi:10.1137/S0036142992228409.

(23) Surhone LM, Timpledon, MT, Marseken, SF. *Monodromy*, Mauritius: Betascript Publishing; 2010.

(24) Van der Aa E, Verhulst F. Asymptotic Integrability and Periodic Solutions of a Hamiltonian System in 1:2:2-Resonance. *SIAM Journal on Mathematical Analysis*. 1984; 15(5):890-911. Available from: https:

//doi.org/10.1137/0515067

(25) Verhulst F. Extension of Poincaré's Program for Integrability, Chaos and Bifurcations. *Chaotic Modeling and Simulation (CMSIM).* 2011; 1:3–16. Available from: https://www.semanticscholar.org/paper/Extension-of-Poincare%27s-program-for-integrability%2C-Verhulst/6837788a73767445f431dc5d2404ab04a3818fe3. [Accessed 14th June 2021]

(26) Van der Aa A. First-Order Resonances in Three-Degrees-of-Freedom Systems. *Celestial Mechanics.* 1983; 31:163–191. Available from: https://doi.org/10.1007/BF01686817.

(27) Lebovitz N. *Stability I: Equilibrium Points.* 2016. Available from: http://people.cs.uchicago.edu/~lebovitz/Eodesbook/stabeq.pdf. [Accessed 14th June 2021]

(28) Woolf P et al. *Using Eigenvalues and Eigenvectors to Find Stability and Solve ODEs*, University of Michigan, 2021. Available from: https://eng.libretexts.org/@go/page/22502. [Accessed 14th June 2021]

(29) Mikhlin Y, Shmatko TV, Manucharyan G. Lyapunov definition and stability of regular or chaotic vibration modes in systems with several equilibrium positions, *Computers and Structures*, 2004; 82(31-32):2733-2742. Available from: https://doi.org/10.1016/j.compstruc.2004.03.082.

(30) Percival IC. Chaos in Hamiltonian Systems, *Proceedings of the Royal Society A* 1987; 413:131-143. Available from: https://doi.org/10.1098/rspa.1987.0105.

(31) Srivastava N, Kaufman C, Müller G. Hamiltonian Chaos *Computers in Physics.* 1990; 4:549-553. Available from: https://doi.org/10.1063/1.4822945

(32) Vitt A, Gorelik G, Shields L. Oscillations of an Elastic Pendulum as an Example of the Oscillations of Two Parametrically Coupled Linear Systems. *Journal of Technical Physics.* 1933; 3:294-307. Available from: http://hdl.handle.net/2262/70474. [Accessed 14th June 2021]

(33) Cushman RH, Dullin HR, Giacobbe A, Holm DD, Joeyeux M, Lynch P, Sadovskii DA, Zhilinksii B. CO_2 Molecule as a Quantum Realization of the 1:1:2 Resonant Swing-Spring with Monodromy. *Physical Review Letters.* 2004; 93(2). DOI: 10.1103/PhysRevLett.93.024302. Available from: https://www.researchgate.net/publication/8388027_C_O_2_Molecule_as_a_Quantum_Realization_of_the_1_1_2_Resonant_Swing-Spring_with_Monodromy

(34) Bretherton FP, Resonant Interactions Between Waves: The Case of Discrete Oscillations. *Journal of Fluid Mechanics.* 1964; 20(3):457-479. Available from: doi:10.1017/S0022112064001355.

(35) Holm DD, Kovačič G. Homoclinic Chaos in a Laser-Matter System. *Physica D: Nonlinear Phenomena*, 1992; 56(2-3):270-300. Available from: https://doi.org/10.1016/0167-2789(92)90029-M.

(36) Alber MS, Luther GG, Marsden JE, Robbins JM, Geometric Phases, Reduction and Lie-Poisson Structure For The Resonant Three-Wave Interaction. *Physica D: Nonlinear Phenomena*. 1998; 123(1-4):271-290. Available from: https://doi.org/10.1016/S0167-2789(98)00127-4.

(37) Lynch P. Replication of Foucault's Pendulum Experiment in Dublin. *Royal Irish Academy, Proceedings of the Royal Irish Academy: Archaeology, Culture, History, Literature* 2016; 116(C):297-311. Available from: doi:10.3318/priac.2016.116.03.

(38) Lynch P. How two Trinity reverends let the great world spin. *The Irish Times*. August 7 2014. Available from: https://www.irishtimes.com/news/science/how-two-trinity-reverends-let-the-great-world-spin-1.1885091. [Acccesed 13th June 2021]

(39) Christov O. *A Note On The Integrability of Hamiltonian 1:2:2 Resonance,* Faculty of Mathematics and Informatics, Sofia University, Sofia, Bulgaria, 2018. Available from https://arxiv.org/pdf/1802.06247.pdf. [Accessed 14th June 2021]

Appendix

Cubic approximation of potential energy of the spring

$$V_s = \frac{kl_0^2}{2}\left(\sqrt{1+\frac{2z}{l_0}+\frac{|\mathbf{x}|^2}{l_0^2}}-1\right)^2 = \frac{kl_0^2}{2}\left(\frac{z}{l_0}+\frac{x^2+y^2+z^2}{2l_0^2}-\frac{z^2}{2l_0^2}-\left(\frac{x^2+y^2+z^2}{8l_0^2}\right)^2-\frac{z(x^2+y^2+z^2)}{2l_0^3}+O\left(\epsilon^3\right)\right)^2 =$$

$$= \frac{kl_0^2}{2}\left(\left(\frac{z}{l_0}\right)^2+\left(\frac{x^2+y^2+z^2}{2l_0^2}\right)^2+\left(\frac{z^2}{2l_0^2}\right)^2+\left(\left(\frac{x^2+y^2+z^2}{8l_0^2}\right)^2\right)^2+\left(\frac{z(x^2+y^2+z^2)}{2l_0^3}\right)^2+O(\epsilon^3)\right)^2 +$$

$$+2\frac{z}{l_0}\frac{x^2+y^2+z^2}{2l_0^2}-2\frac{z}{l_0}\frac{z^2}{2l_0^2}-2\frac{z}{l_0}\left(\frac{x^2+y^2+z^2}{8l_0^2}\right)^2-2\frac{z}{l_0}\frac{z(x^2+y^2+z^2)}{2l_0^3}+2\frac{z}{l_0}O(\epsilon^3)-$$

$$-2\frac{x^2+y^2+z^2}{2l_0^2}\frac{z^2}{2l_0^2}-2\frac{x^2+y^2+z^2}{2l_0^2}\left(\frac{x^2+y^2+z^2}{8l_0^2}\right)^2-2\frac{x^2+y^2+z^2}{2l_0^2}\frac{z(x^2+y^2+z^2)}{2l_0^3}+2\frac{x^2+y^2+z^2}{2l_0^2}O(\epsilon^3)+$$

$$+2\frac{z^2}{2l_0^2}\left(\frac{x^2+y^2+z^2}{8l_0^2}\right)^2+2\frac{z^2}{2l_0^2}\frac{z(x^2+y^2+z^2)}{2l_0^3}-2\frac{z^2}{2l_0^2}O(\epsilon^3)$$

$$+2\left(\frac{x^2+y^2+z^2}{8l_0^2}\right)^2\frac{z(x^2+y^2+z^2)}{2l_0^3}-2\left(\frac{x^2+y^2+z^2}{8l_0^2}\right)^2O(\epsilon^3)-2\frac{z(x^2+y^2+z^2)}{2l_0^3}O(\epsilon^3) =$$

$$= \frac{z^2}{l_0^2}-\frac{z^3}{l_0^3}+\frac{z(x^2+y^2+z^2)}{l_0^3}+o(\epsilon^3) =$$

$$= \frac{z^2}{l_0^2}+\frac{z(x^2+y^2)}{l_0^3}+o(\epsilon^3),$$

as all other terms are of order $o(\epsilon^3)$

Calculation for Averaged Lagrangian of 1:1:2 resonant system

The average Lagrangian is obtained substituting the following relations into $\frac{L}{m}$:

$$x = \Re[a(t)\exp(i\omega_R t)] \qquad y = \Re[b(t)\exp(i\omega_R t)] \qquad z = \Re[c(t)\exp(2i\omega_R t)]$$

obtaining:

$$0.5\lambda\left(\frac{c(t)e^{2i\omega t}}{2}+\frac{e^{-2i\omega t}\overline{c(t)}}{2}\right)\left(\left(\frac{a(t)e^{i\omega t}}{2}+\frac{e^{-i\omega t}\overline{a(t)}}{2}\right)^2+\left(\frac{b(t)e^{i\omega t}}{2}+\frac{e^{-i\omega t}\overline{b(t)}}{2}\right)^2\right)$$

$$-2.0\omega^2\left(\frac{c(t)e^{2i\omega t}}{2}+\frac{e^{-2i\omega t}\overline{c(t)}}{2}\right)^2-0.5\omega^2\left(\left(\frac{a(t)e^{i\omega t}}{2}+\frac{e^{-i\omega t}\overline{a(t)}}{2}\right)^2+\left(\frac{b(t)e^{i\omega t}}{2}+\frac{e^{-i\omega t}\overline{b(t)}}{2}\right)^2\right)$$

$$+0.5\left(\frac{i\omega a(t)e^{i\omega t}}{2}-\frac{i\omega e^{-i\omega t}\overline{a(t)}}{2}+\frac{e^{i\omega t}\frac{d}{dt}a(t)}{2}+\frac{e^{-i\omega t}\frac{d}{dt}\overline{a(t)}}{2}\right)^2$$

$$+0.5\left(\frac{i\omega b(t)e^{i\omega t}}{2}-\frac{i\omega e^{-i\omega t}\overline{b(t)}}{2}+\frac{e^{i\omega t}\frac{d}{dt}b(t)}{2}+\frac{e^{-i\omega t}\frac{d}{dt}\overline{b(t)}}{2}\right)^2$$

$$+0.5\left(i\omega c(t)e^{2i\omega t}-i\omega e^{-2i\omega t}\overline{c(t)}+\frac{e^{2i\omega t}\frac{d}{dt}c(t)}{2}+\frac{e^{-2i\omega t}\frac{d}{dt}\overline{c(t)}}{2}\right)^2$$

This can be further expanded:

$$0.0625\gamma a^2(t)c(t)e^{4i\omega t}+0.0625\gamma a^2(t)\overline{c(t)}+\frac{1}{8}\gamma a(t)c(t)e^{2i\omega t}\overline{a(t)}+\frac{1}{8}\gamma a(t)e^{-2i\omega t}\overline{a(t)c(t)}$$

$$+0.0625\gamma b^2(t)c(t)e^{4i\omega t}+0.0625\gamma b^2(t)\overline{c(t)}+\frac{1}{8}\gamma b(t)c(t)e^{2i\omega t}\overline{b(t)}+\frac{1}{8}\gamma b(t)e^{-2i\omega t}\overline{b(t)c(t)}+0.0625\gamma c(t)\overline{a(t)}^2$$

$$+0.0625\gamma c(t)\overline{b(t)}^2+0.0625\gamma e^{-4i\omega t}\overline{a(t)}^2\overline{c(t)}+0.0625\gamma e^{-4i\omega t}\overline{b(t)}^2\overline{c(t)}-0.25\omega^2a^2(t)e^{2i\omega t}-0.25\omega^2b^2(t)e^{2i\omega t}$$

$$-1.0\omega^2c^2(t)e^{4i\omega t}-0.25\omega^2e^{-2i\omega t}\overline{a(t)}^2-0.25\omega^2e^{-2i\omega t}\overline{b(t)}^2-1.0\omega^2e^{-4i\omega t}\overline{c(t)}^2$$

$$+0.25i\omega a(t)e^{2i\omega t}\frac{d}{dt}a(t)+0.25i\omega a(t)\frac{d}{dt}\overline{a(t)}+0.25i\omega b(t)e^{2i\omega t}\frac{d}{dt}b(t)+0.25i\omega b(t)\frac{d}{dt}\overline{b(t)}$$

$$+0.5i\omega c(t)e^{4i\omega t}\frac{d}{dt}c(t)+0.5i\omega c(t)\frac{d}{dt}\overline{c(t)}-0.25i\omega\overline{a(t)}\frac{d}{dt}a(t)-0.25i\omega\overline{b(t)}\frac{d}{dt}b(t)-0.5i\omega\overline{c(t)}\frac{d}{dt}c(t)$$

$$-0.25i\omega e^{-2i\omega t}\overline{a(t)}\frac{d}{dt}\overline{a(t)}-0.25i\omega e^{-2i\omega t}\overline{b(t)}\frac{d}{dt}\overline{b(t)}-0.5i\omega e^{-4i\omega t}\overline{c(t)}\frac{d}{dt}\overline{c(t)}+\frac{1}{8}e^{4i\omega t}\left(\frac{d}{dt}c(t)\right)^2$$

$$+\frac{1}{8}e^{2i\omega t}\left(\frac{d}{dt}a(t)\right)^2+\frac{1}{8}e^{2i\omega t}\left(\frac{d}{dt}b(t)\right)^2+0.25\frac{d}{dt}a(t)\frac{d}{dt}\overline{a(t)}+0.25\frac{d}{dt}b(t)\frac{d}{dt}\overline{b(t)}+0.25\frac{d}{dt}c(t)\frac{d}{dt}\overline{c(t)}$$

$$+\frac{1}{8}e^{-2i\omega t}\left(\frac{d}{dt}\overline{a(t)}\right)^2+\frac{1}{8}e^{-2i\omega t}\left(\frac{d}{dt}\overline{b(t)}\right)^2+\frac{1}{8}e^{-4i\omega t}\left(\frac{d}{dt}\overline{c(t)}\right)^2$$

As stated in *Section 3.1*, the next step is using our small period assumption, meaning all the terms containing a complex exponential will integrate to zero when calculating the action, so they are negligible in terms of the Euler Lagrange equations and are hence removed. Furthermore, as a, b, c are assumed to vary slowly, terms with a derivative to the second power or higher are also ignored. Hence, the only remaining terms give the Averaged Lagrangian:

$$0.0625\gamma a^2(t)\overline{c(t)} + 0.0625\gamma b^2(t)\overline{c(t)} + 0.0625\gamma c(t)\overline{a(t)}^2 + 0.0625\gamma c(t)\overline{b(t)}^2 + 0.25i\omega a(t)\frac{d}{dt}\overline{a(t)}$$

$$+0.25i\omega b(t)\frac{d}{dt}\overline{b(t)} + 0.5i\omega c(t)\frac{d}{dt}\overline{c(t)} - 0.25i\omega\overline{a(t)}\frac{d}{dt}a(t) - 0.25i\omega\overline{b(t)}\frac{d}{dt}b(t) - 0.5i\omega\overline{c(t)}\frac{d}{dt}c(t)$$

Combining terms with their complex conjugate, the final expression is obtained

$$\langle L\rangle = \frac{1}{2}\omega_R[\Im(\dot{a}a^* + \dot{b}b^* + 2\dot{c}c^*) + \Re(\kappa(a^2+b^2)c^*)]$$

Calculation of the constant of motion N for the 1:1:2 resonance

$$\frac{\partial L}{\partial \dot{a}} = \frac{\omega_R}{2}\frac{\partial}{\partial \dot{a}}\left(\Im(\dot{a}a^*)\right) = \frac{\omega_R}{2}\frac{\partial}{\partial \dot{a}}\left(\frac{\dot{a}a^* - \dot{a^*}a}{2i}\right) = \frac{\omega_R a^*}{4i}$$

$$\frac{\partial L}{\partial \dot{b}} = \frac{\omega_R}{2}\frac{\partial}{\partial \dot{b}}\left(\Im\left(\dot{b}b^*\right)\right) = \frac{\omega_R}{2}\frac{\partial}{\partial \dot{b}}\left(\frac{\dot{b}b^* - \dot{b^*}b}{2i}\right) = \frac{\omega_R b^*}{4i}$$

$$\frac{\partial L}{\partial \dot{c}} = \frac{\omega_R}{2}\frac{\partial}{\partial \dot{c}}\left(2\Im(\dot{c}c^*)\right) = \frac{\omega_R}{2}\frac{\partial}{\partial \dot{c}}\left(\frac{\dot{c}a^* - \dot{c^*}c}{i}\right) = \frac{\omega_R c^*}{2i}$$

We also have that

$$a = \frac{A+B}{\kappa} \implies \dot{a} = \frac{\dot{A}+\dot{B}}{\kappa} \implies \frac{\partial \dot{a}}{\partial \dot{A}} = \frac{1}{\kappa}, \frac{\partial \dot{a}}{\partial \dot{B}} = \frac{1}{\kappa}$$

$$b = \frac{A-B}{i\kappa} \implies \dot{b} = \frac{\dot{A}\dot{B}}{i\kappa} \implies \frac{\partial \dot{b}}{\partial \dot{A}} = \frac{-i}{\kappa}, \frac{\partial \dot{b}}{\partial \dot{B}} = \frac{i}{\kappa}$$

$$c = \frac{C}{\kappa} \implies \dot{c} = \frac{\dot{C}}{\kappa} \implies \frac{\partial \dot{c}}{\partial \dot{C}} = \frac{1}{\kappa}$$

Calculation of the constant of motion K for the 1:1:2 resonance

Our Lagrangian is difference between kinetic and potential energy of the system, so Hamiltonian will be total energy of the system i.e.:

$$H = \frac{1}{2}\left(\dot{x}^2+\dot{y}^2+\dot{z}^2\right) + \frac{1}{2}\left(\omega_R^2\left(x^2+y^2\right)+\omega_Z^2 z^2\right) - \frac{1}{2}\lambda\left(x^2+y^2\right)z = \frac{1}{2}\left(\dot{x}^2+\dot{y}^2+\dot{z}^2\right) + \frac{1}{2}\left(\left(x^2+y^2\right)+4z^2\right) - \frac{1}{2}\lambda\left(x^2+y^2\right)z,$$

as we assume that $\omega_R = 1$ and $\omega_Z = 2$. Substituting

$$x = \Re[a(t)\exp(i\omega_R t)] \qquad y = \Re[b(t)\exp(i\omega_R t)] \qquad z = \Re[c(t)\exp(2i\omega_R t)],$$

we get that

$$H = -0.5\gamma \left(0.5c(t)e^{2i\omega t} + 0.5e^{-2i\omega t}\overline{c(t)}\right)\left(\left(0.5a(t)e^{i\omega t} + 0.5e^{-i\omega t}\overline{a(t)}\right)^2 + \left(0.5b(t)e^{i\omega t} + 0.5e^{-i\omega t}\overline{b(t)}\right)^2\right) +$$

$$+0.5\left(0.5a(t)e^{i\omega t} + 0.5e^{-i\omega t}\overline{a(t)}\right)^2 + 0.5\left(0.5b(t)e^{i\omega t} + 0.5e^{-i\omega t}\overline{b(t)}\right)^2 + 2.0\left(0.5c(t)e^{2i\omega t} + 0.5e^{-2i\omega t}\overline{c(t)}\right)^2 +$$

$$+0.5\left(0.5i\omega a(t)e^{i\omega t} - 0.5i\omega e^{-i\omega t}\overline{a(t)} + 0.5e^{i\omega t}\frac{d}{dt}a(t) + 0.5e^{-i\omega t}\frac{d}{dt}\overline{a(t)}\right)^2 +$$

$$+0.5\left(0.5i\omega b(t)e^{i\omega t} - 0.5i\omega e^{-i\omega t}\overline{b(t)} + 0.5e^{i\omega t}\frac{d}{dt}b(t) + 0.5e^{-i\omega t}\frac{d}{dt}\overline{b(t)}\right)^2 +$$

$$+0.5\left(1.0i\omega c(t)e^{2i\omega t} - 1.0i\omega e^{-2i\omega t}\overline{c(t)} + 0.5e^{2i\omega t}\frac{d}{dt}c(t) + 0.5e^{-2i\omega t}\frac{d}{dt}\overline{c(t)}\right)^2.$$

Expanding all terms we get

$$H = -0.0625\kappa a^2(t)c(t)e^{4i\omega t} - 0.0625\kappa a^2(t)\overline{c(t)} - 0.125\kappa a(t)c(t)e^{2i\omega t}\overline{a(t)} - 0.125\kappa a(t)e^{-2i\omega t}\overline{a(t)c(t)} - 0.0625\kappa b^2(t)c(t)e^{4i\omega t} -$$

$$-0.0625\kappa b^2(t)\overline{c(t)} - 0.125\kappa b(t)c(t)e^{2i\omega t}\overline{b(t)} - 0.125\kappa b(t)e^{-2i\omega t}\overline{b(t)c(t)} - 0.0625\kappa c(t)\overline{a(t)}^2 - 0.0625\kappa c(t)\overline{b(t)}^2 -$$

$$-0.0625\kappa e^{-4i\omega t}\overline{a(t)}^2\overline{c(t)} - 0.0625\kappa e^{-4i\omega t}\overline{b(t)}^2\overline{c(t)} - 0.125\omega^2 a^2(t)e^{2i\omega t} + 0.25\omega^2 a(t)\overline{a(t)} - 0.125\omega^2 b^2(t)e^{2i\omega t} + 0.25\omega^2 b(t)\overline{b(t)} -$$

$$-0.5\omega^2 c^2(t)e^{4i\omega t} + 1.0\omega^2 c(t)\overline{c(t)} - 0.125\omega^2 e^{-2i\omega t}\overline{a(t)}^2 - 0.125\omega^2 e^{-2i\omega t}\overline{b(t)}^2 - 0.5\omega^2 e^{-4i\omega t}\overline{c(t)}^2 + 0.25i\omega a(t)e^{2i\omega t}\frac{d}{dt}a(t) +$$

$$+0.25i\omega a(t)\frac{d}{dt}\overline{a(t)} + 0.25i\omega b(t)e^{2i\omega t}\frac{d}{dt}b(t) + 0.25i\omega b(t)\frac{d}{dt}\overline{b(t)} + 0.5i\omega c(t)e^{4i\omega t}\frac{d}{dt}c(t) + 0.5i\omega c(t)\frac{d}{dt}\overline{c(t)} - 0.25i\omega\overline{a(t)}\frac{d}{dt}a(t) -$$

$$-0.25i\omega\overline{b(t)}\frac{d}{dt}b(t) - 0.5i\omega\overline{c(t)}\frac{d}{dt}c(t) - 0.25i\omega e^{-2i\omega t}\overline{a(t)}\frac{d}{dt}\overline{a(t)} - 0.25i\omega e^{-2i\omega t}\overline{b(t)}\frac{d}{dt}\overline{b(t)} - 0.5i\omega e^{-4i\omega t}\overline{c(t)}\frac{d}{dt}\overline{c(t)} + 0.125a^2(t)e^{2i\omega t}$$

$$+0.25a(t)\overline{a(t)} + 0.125b^2(t)e^{2i\omega t} + 0.25b(t)\overline{b(t)} + 0.5c^2(t)e^{4i\omega t} + 1.0c(t)\overline{c(t)} + 0.125e^{4i\omega t}\left(\frac{d}{dt}c(t)\right)^2 + 0.125e^{2i\omega t}\left(\frac{d}{dt}a(t)\right)^2 +$$

$$+0.125e^{2i\omega t}\left(\frac{d}{dt}b(t)\right)^2 + 0.25\frac{d}{dt}a(t)\frac{d}{dt}\overline{a(t)} + 0.25\frac{d}{dt}b(t)\frac{d}{dt}\overline{b(t)} + 0.25\frac{d}{dt}c(t)\frac{d}{dt}\overline{c(t)} + 0.125e^{-2i\omega t}\overline{a(t)}^2 + 0.125e^{-2i\omega t}\overline{b(t)}^2 +$$

$$+0.125e^{-2i\omega t}\left(\frac{d}{dt}\overline{a(t)}\right)^2 + 0.125e^{-2i\omega t}\left(\frac{d}{dt}\overline{b(t)}\right)^2 + 0.5e^{-4i\omega t}\overline{c(t)}^2 + 0.125e^{-4i\omega t}\left(\frac{d}{dt}\overline{c(t)}\right)^2.$$

After cancelling terms with exponential and derivatives to the second power in the same way as when calculating the averaged Lagrangian we get that the averaged Hamiltonian is

$$< H >= \frac{|a|^2}{2} + \frac{|b|^2}{2} + 2|c|^2 - \frac{\lambda}{8}\frac{a^2c^* + a^{*2}c}{2} - \frac{\lambda}{8}\frac{b^2c^* + b^{*2}c}{2} + \frac{i}{2}\left(\frac{a\dot{a}^* - a^*\dot{a}}{2} + \frac{b\dot{b}^* - b^*\dot{b}}{2}\right) + i\frac{c\dot{c}^* - c^*\dot{c}}{2} =$$

$$= \frac{|a|^2}{2} + \frac{|b|^2}{2} + 2|c|^2 - \frac{\lambda}{8}\Re((a^2 + b^2)c^*) - \frac{\Im(a\dot{a}^* + b\dot{b}^* + 2c\dot{c}^*)}{2}$$

Note that

$$|A^2| + |B|^2 + 2|C|^2 = \frac{\kappa^2}{4}\left((a + ib)(a^* - ib^*) + (a - ib)(a^* + ib^*)\right) + 2\kappa^2|c|^2 = \kappa^2\left(\frac{|a|^2}{2} + \frac{|b|^2}{2} + 2|c|^2\right)$$

is constant, hence $\frac{|a|^2}{2} + \frac{|b|^2}{2} + 2|c|^2$ is as well.

Furthermore, using the Euler-Lagrange equations for a, b, c we find that

$$\dot{a}a^* + \dot{b}^* - 4\dot{c}c^* = \frac{\kappa}{i}\left((a^{*2} + b^{*2})c - (a^2 + b^2)c^*\right) = 2\kappa\Im((a^{*2} + b^{*2})c) \implies \Im(\dot{a}a^* + \dot{b}^* - 4\dot{c}c^{)} = 0 \implies$$

$$\implies \Im(\dot{a}a^* + \dot{b}^* + 2\dot{c}c^*) = \Im(6\dot{c}c^*) = \Im\left(\frac{6}{i}\frac{\kappa(a^2 + b^2)c^*}{4}\right) = \frac{3\kappa}{2}\Re\left((a^2 + b^2)c^*\right)$$

Derivation of initial conditions for the Slowly Varying Envelope Equations

The expressions for the initial conditions of the SVE equations can be derived in the following manner. First by assume

$$x(t) = |a(t)|\cos(\omega_R t + \alpha)$$

assuming α is constant and substituting $t = 0$ we will have

$$x_0 = |a_0|\cos\alpha_0$$

taking derivatives and upon substitution

$$\dot{x}_0 = -w_R|a_0|\sin(\alpha_0)$$

and use the above equations to solve for $|a_0|$ (whichever initial condition is non zero will determine which particular equation we use). Similar equations work for y and z using the appropriate angles and frequency

values. For the initial phase, we exploit both of the above equations, dividing them to get

$$\frac{x_0}{\dot{x}_0} = -\frac{\cos\alpha_0}{\omega_R \sin\alpha_0}$$

yielding the aforementioned equation. Furthermore, for all other coordinates analogous derivations will work.

Calculation for Averaged Lagrangian of 1:2:2 resonant system

Using the same substitution as before, adapted for the new resonance:

$$x = \Re[a(t)\exp(i\omega t)] \qquad y = \Re[b(t)\exp(i2\omega t)] \qquad z = \Re[c(t)\exp(2i\omega t)]$$

and plugging this into the Lagrangian L_{122} and expanding all the terms we get:

$$\frac{a_1 a^2(t) b(t) e^{4i\omega t}}{8} + \frac{a_1 a^2(t)\overline{b(t)}}{8} + \frac{a_1 a(t) b(t) e^{2i\omega t}\overline{a(t)}}{4} + \frac{a_1 a(t) e^{-2i\omega t}\overline{a(t)b(t)}}{4} + \frac{a_1 b(t)\overline{a(t)}^2}{8} + \frac{a_1 e^{-4i\omega t}\overline{a(t)}^2\overline{b(t)}}{8}$$

$$+\frac{a_2 a^2(t) c(t) e^{4i\omega t}}{8} + \frac{a_2 a^2(t)\overline{c(t)}}{8} + \frac{a_2 a(t) c(t) e^{2i\omega t}\overline{a(t)}}{4} + \frac{a_2 a(t) e^{-2i\omega t}\overline{a(t)c(t)}}{4} + \frac{a_2 c(t)\overline{a(t)}^2}{8} + \frac{a_2 e^{-4i\omega t}\overline{a(t)}^2\overline{c(t)}}{8}$$

$$-\frac{1}{8}\omega^2 a^2(t) e^{2i\omega t} + 0.25\omega^2 a(t)\overline{a(t)} - 0.5\omega^2 b^2(t) e^{4i\omega t} + 1.0\omega^2 b(t)\overline{b(t)} - 0.5\omega^2 c^2(t) e^{4i\omega t} + 1.0\omega^2 c(t)\overline{c(t)}$$

$$-\frac{1}{8}\omega^2 e^{-2i\omega t}\overline{a(t)}^2 - 0.5\omega^2 e^{-4i\omega t}\overline{b(t)}^2 - 0.5\omega^2 e^{-4i\omega t}\overline{c(t)}^2 + 0.25 i\omega a(t) e^{2i\omega t}\frac{d}{dt}a(t) + 0.25 i\omega a(t)\frac{d}{dt}\overline{a(t)}$$

$$+0.5 i\omega b(t) e^{4i\omega t}\frac{d}{dt}b(t) + 0.5 i\omega b(t)\frac{d}{dt}\overline{b(t)} + 0.5 i\omega c(t) e^{4i\omega t}\frac{d}{dt}c(t) + 0.5 i\omega c(t)\frac{d}{dt}\overline{c(t)} - 0.25 i\omega\overline{a(t)}\frac{d}{dt}a(t) - 0.5 i\omega\overline{b(t)}\frac{d}{dt}b(t)$$

$$-0.5 i\omega\overline{c(t)}\frac{d}{dt}c(t) - 0.25 i\omega e^{-2i\omega t}\overline{a(t)}\frac{d}{dt}\overline{a(t)} - 0.5 i\omega e^{-4i\omega t}\overline{b(t)}\frac{d}{dt}\overline{b(t)} - 0.5 i\omega e^{-4i\omega t}\overline{c(t)}\frac{d}{dt}\overline{c(t)} - \frac{1}{8}a^2(t) e^{2i\omega t}$$

$$-0.25 a(t)\overline{a(t)} - 0.5 b^2(t) e^{4i\omega t} - 1.0 b(t)\overline{b(t)} - 0.5 c^2(t) e^{4i\omega t} - 1.0 c(t)\overline{c(t)} + \frac{1}{8}e^{4i\omega t}\left(\frac{d}{dt}b(t)\right)^2 + \frac{1}{8}e^{4i\omega t}\left(\frac{d}{dt}c(t)\right)^2$$

$$+\frac{1}{8}e^{2i\omega t}\left(\frac{d}{dt}a(t)\right)^2 + 0.25\frac{d}{dt}a(t)\frac{d}{dt}\overline{a(t)} + 0.25\frac{d}{dt}b(t)\frac{d}{dt}\overline{b(t)} + 0.25\frac{d}{dt}c(t)\frac{d}{dt}\overline{c(t)} - \frac{1}{8}e^{-2i\omega t}\overline{a(t)}^2$$

$$+\frac{1}{8}e^{-2i\omega t}\left(\frac{d}{dt}\overline{a(t)}\right)^2 - 0.5 e^{-4i\omega t}\overline{b(t)}^2 - 0.5 e^{-4i\omega t}\overline{c(t)}^2 + \frac{1}{8}e^{-4i\omega t}\left(\frac{d}{dt}\overline{b(t)}\right)^2 + \frac{1}{8}e^{-4i\omega t}\left(\frac{d}{dt}\overline{c(t)}\right)^2$$

Now, proceeding as for the 1:1:2 case, terms with a complex exponential multiple are neglected as they will integrate to zero when calculating the action, and furthermore, non-dimensionalising the problem so that

$\omega = 1$, the terms that remain are the following:

$$\frac{a_1 a^2(t)\overline{b(t)}}{8}+\frac{a_1 b(t)\overline{a(t)}^2}{8}+\frac{a_2 a^2(t)\overline{c(t)}}{8}+\frac{a_2 c(t)\overline{a(t)}^2}{8}+\frac{i a(t)\overline{\dot{\mathrm{a}}\,(t)}}{4}-\frac{i\,\dot{\mathrm{a}}\,(t)\overline{a(t)}}{4}+\frac{i b(t)\overline{\dot{\mathrm{b}}\,(t)}}{2}-\frac{i\,\dot{\mathrm{b}}\,(t)\overline{b(t)}}{2}+\frac{i c(t)\overline{\dot{\mathrm{c}}\,(t)}}{2}-\frac{i\,\dot{\mathrm{c}}\,(t)\overline{c(t)}}{2}$$

Combining them we get the final form of the Averaged Lagrangian

$$\langle L\rangle = \frac{\Im[\dot{a}a^* + 2\dot{b}b^* + 2\dot{c}c^*]}{2} + \frac{\Re[a^2(a_1 b^* + a_2 c^*)]}{4}$$